Friction Stir Welding of Austenitic Stainless Steel (AISI-316) to Ti-6Al-4V and its Joint Analyses

Manish Purushottam Meshram

A Dissertation Submitted to

Indian Institute of Technology Hyderabad

In Partial Fulfillment of the Requirements for

The Degree of Master of Technology

भारतीय प्रौद्योगिकी संस्थान हैदराबाद
Indian Institute of Technology Hyderabad

Department of Materials Science and Metallurgical Engineering

June 2014

Declaration

I declare that this written submission represents my ideas in my own words, and where others' ideas or words have been included, I have adequately cited and referenced the original sources. I also declare that I have adhered to all principles of academic honesty and integrity and have not misrepresented or fabricated or falsified any idea/data/fact/source in my submission. I understand that any violation of the above will be a cause for disciplinary action by the Institute and can also evoke penal action from the sources that have thus not been properly cited, or from whom proper permission has not been taken when needed.

_____

(Signature)

Manish Purushottam Meshram

(– Student Name –)

MS12M1007

(Roll No)

Approval Sheet

This thesis entitled Friction Stir Welding of Austenitic Stainless Steel (AISI-316) to Ti-6Al-4V and its Joint Analyses by Manish Purushottam Meshram is approved for the degree of Master of Technology from IIT Hyderabad.

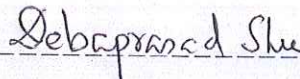Dr. Bharat Bhooshan Panigrahi (Assistant Professor)

Examiner

Dr. Atul Suresh Deshpande (Assistant Professor)

Examiner

Dr. Suhash Ranjan Dey (Assistant Professor)

Adviser

Dr. Debaprasad Shee (Assistant Professor)

Chairman

Acknowledgements

Dedicated

To

My Parents

My Father Mr. Purushottam Meshram

My Mother Mrs. Kusum Purushottam Meshram

Abstract

In this project, possibility of joining dissimilar AISI-316 stainless steel to Ti-6Al-4V by friction stir welding was studied. Firstly, similar plates of AISI-316 stainless steel were welded using PCBN tool. Secondly similar plates of Ti-6Al-4V were welded using the same tool. All welds were mechanically tested by tensile strength, hardness measurement and microstructural studies had been carried using optical microscopy and EBSD analysis.

A defect free weld of AISI-316 was obtained with welding parameters of rotation speed 1100 RPM and welding speed of 8 mm/min. Ultimate tensile strength of this welded sample was obtained just above the base material with an increase in hardness in the nugget zone. In EBSD analysis of stir zone C {001} <110> shear component in the stir zone (except for B {hkl} <110> partial fiber in Region 2) in the present low stacking fault stainless steel indicates predominant shear texture along the <110> direction.

At 800 RPM and 50mm/min welding speed defect free weld of Ti-6Al-4V was obtained. In Nugget Zone, Widmanstätten secondary α laths in the matrix β phase grains, indicating its phase transformation from the high temperature β region. TMAZ consisted of deformed α grains and β transformed secondary laths, indicating its operation in the α+β region. D_2 {-1-12} <111> shear texture was observed in Stir Zone of Ti-6Al-4V welds. Ti-6Al-4V welds have shown around 75% of weld strength as compared to base material with minimal elongation of 2 %. This clearly shows non-feasible welding of Ti-6Al-4V with Q70 Megastir tool.

Nomenclature

FSW - Friction Stir Welding

RPM – Rotation per Minute

WS – Welding Speed

PD – Plunge Depth

NG – Nugget Zone

SZ – Stir Zone

TMAZ – Thermomechanically Affected Zone

HAZ – Heat Affected Zone

BM – Base Material

VHN – Vickers Hardness Number

MTS – Material Testing System

UTS – Ultimate Tensile Strength

OM – Optical Microscopy

TA – Tensile Axis

ND – Normal Direction

WD – Welding Direction

SEM – Scanning Electron Microscopy

FEG – Field Emission Gun

OIM – Orientation Image Mapping

EBSD – Electron Backscattered Diffraction

PF – Pole Figure

IPF – Inverse Pole Figure

Contents

List of Figures

List of Tables

Chapter 1

INTRODUCTION

1.1 Joining

Joining is one of the essential manufacturing processes used to bring several components together to make single functional entity. In complex manufacturing processes, joining is one of the last processes. Joining of materials is very essential in our day to day life as it decreases overall the cost of whole assembly [1]. Different kind of joining processes are shown in fig1.
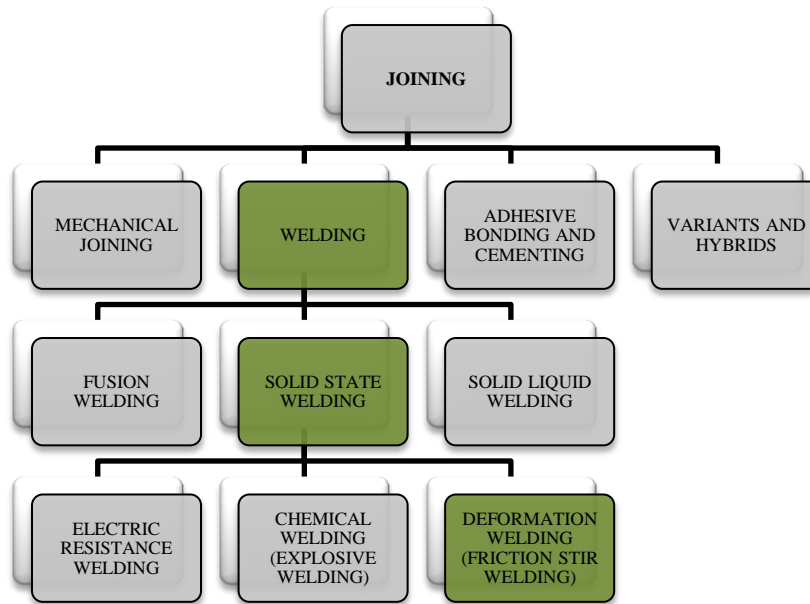
Figure 1: Flow chart of various kind of joining processes.

1.1.1 WELDING

Welding is an effective and versatile process for joining similar and dissimilar types of materials, including metals and nonmetals. It uses the combination of heat and pressure to bring material in plasticize state for solid state joining. The welding processes are broadly classified as fusion welding and solid state welding depending on whether melting or plastic deformation is the principle means for bringing atoms, ions, or molecules together to affect weld. In Fusion welding, peak temperature reached in the weld zone is the melting point of material yields casted structure in weld zone and wide heat affected zone (HAZ) resulted in high level of solidification related defects, strength reduction and distortion [2]. On the other hand, FSW is a solid state joining process in which the maximum temperature attained in weld zone is well below melting point of material hence most of the solidification related defects are eliminated and reduced residual stresses, distortion.

General problems associated with fusion welding are -:

1) Poor mechanical properties due to melting and recasting structure in weld zone.
2) High residual stresses and distortion.
3) Inclusions of hydrogen, nitrogen and oxygen in weld.
4) Poor fatigue, corrosion, and stress corrosion cracking performance.
5) Expensive consumable filler material required.
6) High energy consumption.

Depending upon application FSW was chosen over Fusion welding

1.1.1.1 Friction Stir Welding

Friction stir welding (FSW) is a solid state joining process invented and patented by The Welding Institute (TWI, UK) [3]. Initially, FSW was applied on Aluminum and its alloys as it's very difficult to weld them by conventional methods. The first commercial application of friction stir welding concerned the manufacture of hollow

2

aluminum panels for deep freezing of fish on fishing boats in November 1996 at Sapa in Finspång (Sweden) [4].

1.1.1.1.1 Principle of Operation

There are four different stages in the operation of FSW. (a) Plunge stage (b) Dwell stage (c) weld stage (d) Retraction stage. Firstly, a non-consumable rotating tool with a specially designed pin and shoulder was inserted into the abutting edges of sheets or plates to be joined. Secondly shoulder of the tool touching to plate surface was rotated for some time with enough rotation to generate heat due to friction which softens the material beneath it. Thirdly, tool was traversed along the line of joint during this the localized heating softens the material around the pin and combination of tool rotation and translation leads to movement of material from the front of the pin to the back of the pin. As a result of this process a joint is produced in 'solid state' and finally tool was retracted slowly. The whole process is diagrammatically explained in fig 2. Tool serves two primary functions: (a) heating of work piece, and (b) movement of material to produce the joint. Because of various geometrical features of the tool, the material movement around the pin can be quite complex. The side of the material where the welding direction and tool rotation direction are same is called advancing side (AS) and the side where it is opposite is called retreating side (RS). During FSW process, the material undergoes intense plastic deformation at elevated temperature, resulting in generation of fine and equiaxed recrystallized grains. The fine microstructure in friction stir welds produces good mechanical properties [5].
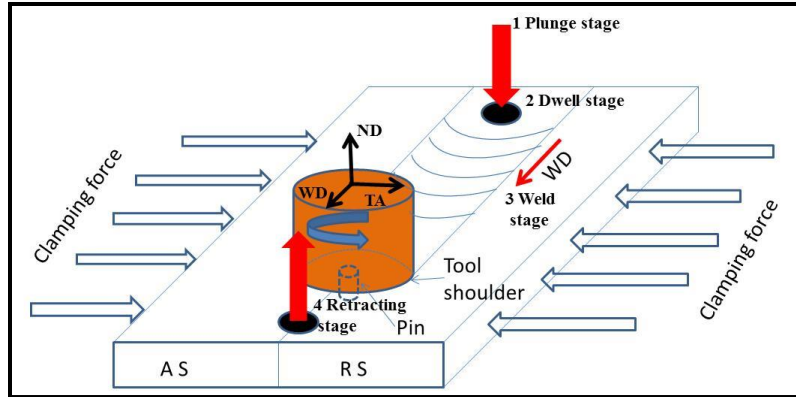
Figure 2: Schematic of Friction Stir Welding

Various stages in FSW

    a) Plunge Stage

    b) Dwell Stage

    c) Weld Stage

    d) Retracting Stage

1.1.1.1.2 Process Parameters

Excellent weld quality with minimum welding defects and reduced tool wear is what required making FSW commercially applicable in industry. To achieve this, process parameters are to be designed efficiently.

Major process parameters to be controlled as follows-:

    a) Rotations Per Minute (RPM)

    b) Welding Speed (mm/min)

    c) Welding Forces

    d) Tool Tilt Angle

    e) Plunge Depth (mm)

Rotation Per Minute (RPM)

RPM is one of the most crucial parameter of FSW which decides heat generation, stirring and mixing of material around rotating pin during weld. In order to produce a successful weld it is necessary that the material surrounding the tool is hot enough to enable the extensive plastic flow required and minimize the forces acting on the

4

tool. If rotation speed is high it create void in the upper surface due to release of stirred material in the FSW zone but if rotation speed is less proper mixing will not take place due to lack of stirring action by tool pin.

Welding Speed

Welding speed is defined as traversing of the tool along weld line during welding. It is the second important parameter which decides the weld quality. With same RPM if welding speed is high then it yield cold weld on the other if weld speed is low then it gives hot weld. Generally lower welding speed gives higher strength to weld.

Welding Forces

There are a number of forces that act on the tool during welding and are given below:

(i) Downwards force: A downwards force is essential to maintain the position of the tool at or below the material surface. This force increase when tool is plunged into the material or mainly when shoulder touches the work piece.

(ii) Traverse force: The traverse force acts parallel to the tool motion and is positive in the welding direction. Since this force arises as a result of the resistance of the material to the motion of the tool

(iii) Lateral force: The lateral force may act perpendicular to the tool traverse direction and is defined here as positive towards the advancing side of the weld.

(iv) Torque: Torque is required to rotate the tool, the amount of which will depend on the downward force and friction coefficient (sliding friction) and/or the flow strength of the material in the surrounding region (sticking friction).

Tool Tilt Angle

Tilting of FSW tool during welding is nothing but creating an angle between normal direction of work piece and tool axis. Tilting provides pressing of plasticized material behind the tool while traversing. Mostly, tool tilt angle is maintained between 0 to 3 degrees. FSW of austenitic steel with a WC-Co tool showed an

optimum tilt angle at 2 degrees, which increased the joint strength with up to 70 % in comparison with the value at a tilt angle of 0 degrees [7].

Plunge Depth

Plunge depth is defined as the depth of the lowest point of the shoulder below the surface of the weld plate and this helps to ensure sufficient forging of the material at the rear of the tool. The FSW tool is tilted backward with respect to the weld line to avoid the material removal from the leading edge by the edge of the shoulder. Plunge depth should be optimized in such a way that there will be minimal flash generation.

1.1.1.1.3 Tool Design

Welding tool depth in work piece is important factor to improve weld quality. There are two aspects to this requirement explained schematically in fig 3 with eq. 1

(i) Welding tool shoulder contact with the work piece surface must be regulated to give consistent heat generation and weld consolidation.

(ii) The welding tool pin depth must be controlled to maintain close proximity to the anvil [8].
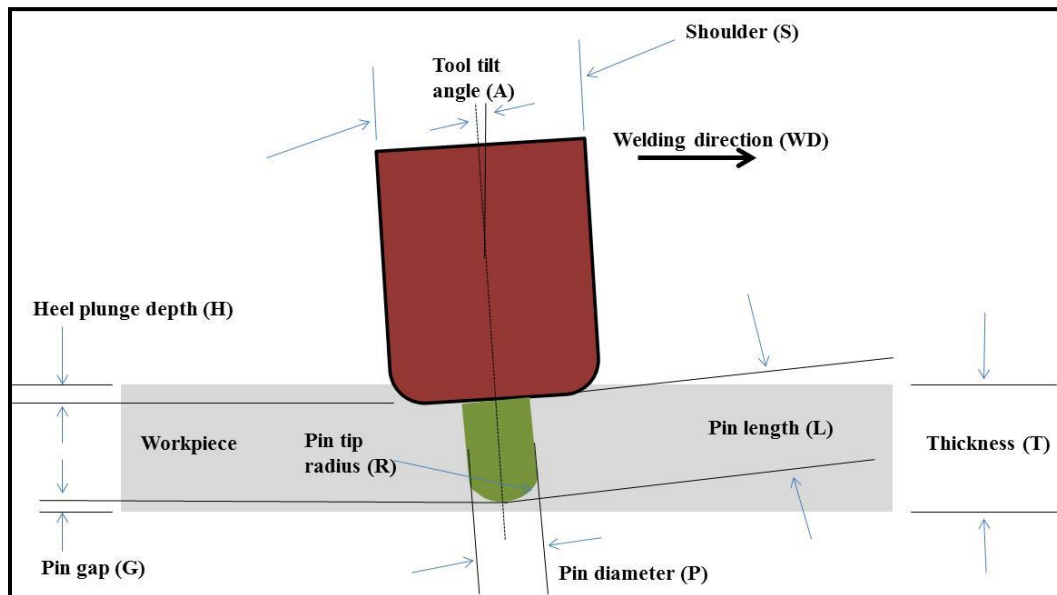
Figure 3: Schematic of FSW Tool

Equation for calculating the pin length for rounded bottom pin,

6

$$L = R + \frac{T-G-H-R+\frac{s}{2}\sin A}{\cos A} \text{...........................} \text{Equation (1)}$$

Where, H can be calculated as below,

$$H = 0.7 * \sin A$$

1.1.1.1.4 Tool Material

FSW is a thermomechanical deformation process where the tool temperature approaches the workpiece solidus temperature. Tool is the prime component which needs to be intact from the start to end of the weld to ensure the quality of a weld. The simple material selection criterion can be taken as "the yield strength of the tool material should be higher than the forces arise during welding". All friction stir tools contain features designed for a specific function. Thus, it is undesirable to have a tool that loses dimensional stability, the designed features, or fractures. For selecting tool material following material characteristics should be considered [9].

- (i)   Ambient and Elevated temperature strength
- (ii)   Elevated temperature stability
- (iii)   Wear Resistance
- (iv)   Tool Reactivity
- (v)   Fracture Toughness
- (vi)   Coefficient of Thermal Expansion
- (vii) Thermal Conductivity

1.1.1.1.5 Heat Generation and Distribution

According to Numerical three-dimensional heat flow model developed by Frigaad et al. for friction stir welding of age hardenable aluminum alloy, the average heat input per unit area and time mostly depends on RPM and tool shoulder. The equation is given below,

$$Q = \frac{4}{3}\pi^2 \mu P \omega R^3 \text{...................................} \text{Equation 2}$$

Where,

Q - Net power (watt)

μ- Frictional Coefficient

P – Pressure (Pa)

ω – Tool Rotation (RPM)

R – Shoulder radius (mm)

To obtain a sound depression free weld nugget the pressure P cannot exceed the actual flow stress of the material at the operating temperature [10]. Three-dimensional thermal model based on finite element analysis developed by Chao and Qi suggested that the peak temperature observed in weld nugget and it goes on decreasing with increase in weld speed [11]. The temperature at advancing side is higher as compare to retreating side. The maximum temperature is observed to be a strong function of the rotation rate (RPM) while the rate of heating is a strong function of the welding speed (mm/min) [12].

1.1.1.1.6 Weld Microstructure

There are specifically four different zones in the welded specimen

(i) Nugget Zone / Weld zone – It is a zone where actual welding of material takes place due to stirring of plasticized material. This central weld zone fully recrystallized consists of fine equiaxed grains. The stir zone or nugget is subjected to the greatest strain and strain rates, as well as the highest temperatures. This combination of parameters apparently results in dissolution of strengthening precipitates as well as continuous dynamic recrystallization.

(ii) Thermomechanically Affected Zone - Region exactly next to weld nugget plastically deformed by FSW tool. It's very difficult to find boundary between HAZ and TMAZ.

(iii) Heat Affected Zone – This zone affected by heat which leads to grain growth of the initial base material grains.

(iv) Base material – This region remains completely unaffected microstructurally [13].
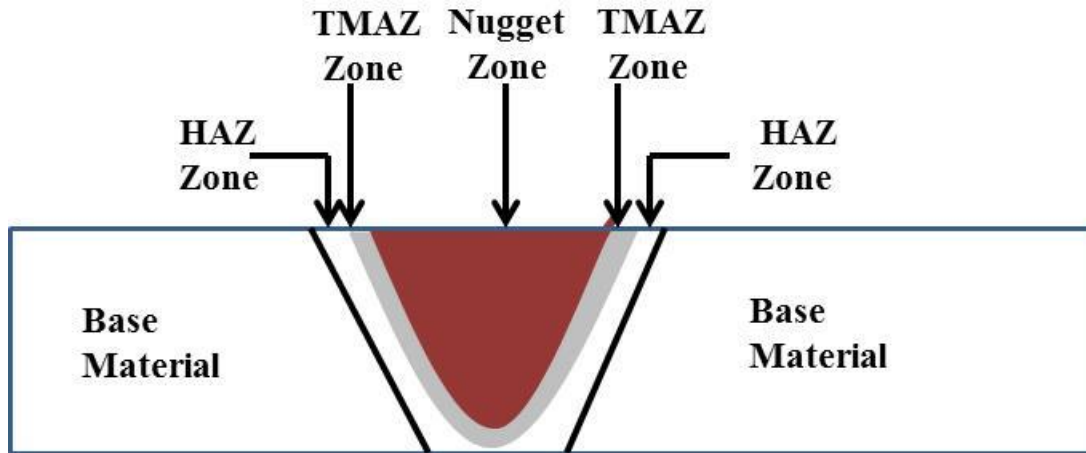
Figure 4: Various zones in Friction stir welded sample

1.1.1.1.7 Advantages and Disadvantages

Maximum output, better quality with minimum input is the need to make any process applicable in industry. FSW of aluminum alloys have fulfilled many requirements like energy efficiency, clean technology as compare to other welding techniques, thus it is commercially applicable in many industries.

Advantages

1) FSW may weld any material irrelevant to the chemistry of material (dissimilar material joining).

2) Due to solid state nature processing temperature is less than fusion welding which decreases energy consumption and eliminates casting structure, porosity and cracking in weld.

3) Reduced distortion and residual stresses in weld.

4) Autogenous process as it does not require any consumables like costly filler material or shielding gases.

5) Better mechanical properties in weld region due to reduced HAZ and finer grains in weld nugget.

There are few limitations and special requirements of FSW and are mentioned below.

9

Disadvantages

1) Non consumable tool for hard materials like steel and titanium is difficult and costly to manufacture.

2) To clamp the work piece materials firmly suitable backing bars are needed to prevent the abutting of plates from moving during welding.

3) Exit whole remains when the tool is withdrawn.

4) Initial cost to setup the equipment is high.

Chapter 2

Literature Survey

2.1 On FSW of Steel

Initially FSW was applied to soft low melting point metals like Aluminum alloys [2]. It is very difficult to weld materials having high melting (softening) temperature by FSW, due to unavailability of nonconsumable rotating tool. In the year 1998, PCBN and tungsten alloys were developed to produce FSW tool which were having ability to withstand high temperature and stresses generated during FSW. C. Meran et al. friction stir welded 2.5 mm thick plates of AISI 304 by tungsten based alloy tool with constant RPM of 1000 and varying WS from 40 to 100 mm/s [13]. The best welding appearance was obtained when the tool dipping angle was 1.45^{o} The least waiting time for pre-heating was determined to be 45 second for the welding conditions of 1000 rpm rotating speed, 63 mm/min travelling speed, and 1.45 tool dipping angle. HAZ was also not observed in the microstructural characterization [14]. Friction stir welding of steel pipes were carried out using PCBN tools with 25 mm in diameter and 5.5 mm in length by applying 500 – 600 rpm rotational speed and 100 -150 mm/min welding speed. Different from similar studies, compressive tool force, that is a very important parameter for friction stir welding, has been kept constant at 10 kN during welding. In order, to prevent oxidation of the weld zone, a protecting argon gas atmosphere is necessary to cover the welding bead [15]. E.

Almanza-Casas et al. successfully friction stir welded 304L-304L and 316L-316L stainless steel plates by using a pin known as Q-60 (60 % PCBN and 40 % WRe). Welding parameters used are 200 RPM and WS 2.5 inches/min [16]. AISI 304L stainless steel sheets of thickness 3.2 mm were joined by friction stir welding using tungsten alloy tool at a single welding speed of 1.7 mm/s using two different tool rotation rates 300 and 500. The resulting welds were overmatched relative to the base metal. Longitudinal residual stresses (tensile) were near the base metal yield strength [17]. 6 mm thick AISI 304 stainless steel plates were friction stir welded by PCBN tool with RPM of 550 and WS of 1.3 mm/s. Rapid formation of sigma phase was observed in welds. A possibility was suggested that the sigma formation can be accelerated by the emergence of delta-ferrite at high temperature and the subsequent decomposition of the ferrite under the high strain and recrystallization induced by friction stirring [18]. Super duplex stainless steel SAF 2507 plates of thickness 4 mm were friction stir welded at 450 RPM and WS of 1mm/s using PCBN tool. Dynamic recrystallization of ferrite and austenite phase yields very fine grains in nugget zone leads to excellent mechanical strength roughly same as base material [19].

2.2 On FSW of Titanium

Titanium alloys (example Ti-6Al-4V) are light weight high melting point temperature non-ferrous material having broad application in high performance aerospace structures. Furthermore due to its excellent corrosion resistance ability in various environments it is being used in many chemical industries, power plants and medical appliances [19]. Welding of Titanium alloys by conventional method have various drawbacks such as high reactivity above 500°C, more prone to dissolve gases like hydrogen, oxygen and nitrogen in liquid state, hence welding must be carried out in inert atmosphere. High temperature in weld zone leads to coarse grain structure in both weld zone and HAZ results in decrease in ductility [20]. Maximum temperature in weld zone of FSW is predicted to be around 0.8 of melting

temperature of material gives lesser defects [21]. FSW is easily applicable to low melting temperature materials like Aluminum alloys as nonconsumable rotating required for them was cheaply available, hence it applicable commercially. But FSW of hard materials like Ti-6Al-4V is a challenging task, as it's difficult to develop a suitable FSW tool. Materials like Tungsten alloy and PCBN are designed to develop FSW tool for such hard materials which are meant to withstand high temperature processing but they are very costly [22, 23]. S. Mironov et al. friction stir welded 2 mm thick plates of Ti-6Al-4V at 500 rpm tool rotational speed and 60 mm/min welding speeds using a convex shoulder Mo-based alloy tool. Argon was the shielding gas to minimize surface oxidation [24]. WC-6wt%Co tool was used by Kumar et. al. to successfully weld 6.4 mm thick Ti-6Al-4V plates. The weld was done at 1000 rpm, with a travel speed of 25.4 mm/min showed improvements in Tensile strength (about 31%) and hardness compared to the parent material [25].

Inference from Literature Survey

1) For FSW of Stainless Steel many researchers used various tool materials like W-Co alloy, W-Re alloys, W-carbides, Mo-based alloys, PCBN and PCBN-WRe. FSW parameters RPM varied from 200 to 1000 and welding speed altered from 20 mm/min to 150 mm/min also tool tilt angle varied from 0° to 3°.

2) For FSW of Ti-alloys tool materials like W-alloys, PCBN, W-carbides alloys were used with varying welding parameters like RPM from 400 to 1000 and welding speed 25 mm/min to 100 mm/min.

Chapter 3

Equipment's Used

3.1 For Friction Stir Welding

3.1.1 ETA Friction Stir Welding Machine

Three axis control FSW facility at IISc Banglore (Professor Satish V. Kailas's laboratory) was used to manufacture welds. Machine consist of data acquisition system for normal load, torque, traverse load, plunge and traverse movement with provision to weld with variable rpm, tool weld speed and plunge depth. Specifications are given in the following table.

Table1: ETA FSW machine specifications

	Min.	Max
Spindle speed	1 RPM	3000 RPM
Welding speed	16 µm/sec	3000 mm/min
Plunge speed	16 µm/sec	2000 mm/min

Figure 5: ETA FSW facility at IISc Banglore

3.2 For Characterization
3.2.1 Grinding Machine

German made twin wheel SAPHIR 330 Grinder and Polisher was used to prepare samples for metallography. For grinding purpose 180, 600, 1200, 2000 grit emery paper were used with water cooling simultaneously. EDM cut samples of size 40

mm x 3 mm x 4 mm were grinded from transverse side to obtain fine surface prepared for OM, SEM and Vickers hardness analysis.

Figure 6 Grinding machine

3.2.2 Automatic Polishing Machine

Tegram automatic polisher and DiaDuo-2 water based diamond polishing suspension (DPS) of 9µm, 6µm, 3µm and 1µm provided by Struers was used to get mirror finish polishing and minimum scratches. DPS can be supplied manually or automatically as per requirement.

Figure 7: Automatic polishing machine

3.2.3 Electropolishing and Etching Machine

Struers Lectropol 5® was used for electropolishing of the specimens used for characterization. Electropoling and etching plays a crucial role in optical and scanning electron microscopy. Scanning function was used to optimize exact voltage for electropolishing and etching of samples from current density graph avoiding tedious permutations and combination.

Figure 8 Lectropol 5 electropolishing machine

Once the voltage was optimized other parameters like flow rate, time and temperature were fined tuned to get best results for electropolishing. A3 electrolyte solution was used at around $0^{o}C$ for stainless steel and Ti-6Al-4V.

3.2.4 Optical Microscope

Leica DM 6000M with Leica Application Suite (LAS) was used for optical microscopy of transverse section of welded samples. System consists of various magnifications of 5x, 10x, 20x, 50x with fully automated stage.

Figure 9: Optical Microscope

3.2.5 Microhardness Measuring Machine

Dura Scan 20 Emco-Test Vickers hardness machine with diamond pyramid shaped indenter was used to get hardness profile. It has one lens and two magnification system 10x and 40x. EN ISO 6507, ASTM E-384 specification were followed while taking measurements.

Figure 10: Microhardness measuring machine

3.3.6 Scanning Electron Microscope

A focused beam of electrons was used to scan the sample during this electrons interact with atoms in the sample, producing various signals that can be detected which contain information about the sample's surface topography and composition. The electron beam is generally scanned in a raster scan pattern, and the beam's position is combined with the detected signal to produce an image. The microstructure and texture were measured using Electron Backscatter Diffraction (EBSD) system (Oxford Instruments, UK) attached to a FEG-SEM (Carl-Zeiss, Model: Supra40). The acquired EBSD data was analyzed using HKL and TSL-OIM™ analysis software.

Figure 11: Scanning electron microscope

EBSD is a microstructural-crystallographic characterization technique used to examine the crystallographic orientation of crystalline materials, used to determine their texture or preferred orientation. A source of electron beam when focused on a thick crystalline material, electron backscattered diffraction pattern also called Kikuchi pattern is generated which is then acquired by the camera and matched with the computer generated Kikuchi pattern of the input crystal system specification by the software and the crystal orientation is determined. When this step is repeated after regular interval of distance while scanning over the specimen surface, an orientation image map containing variety of crystallographic details is obtained.

3.3.7 Universal Testing Machine

Two tensile testing machines one MTS with capacity of 100 KN load cell for high strength Ti-6Al-4V and second one of Instron with 30 KN load cell for AISI- 316 stainless steel were used to obtain mechanical properties of welds.

Figure 12: MTS universal testing machine

Figure 13: Instron tensile testing machine

18

Both machines were used to obtain various mechanical properties like Yield strength and Ultimate tensile test. As stainless steel has lower strength than Ti-6Al-4V Instron testing machine with low capacity load cell was used for better precision and accuracy. Dog bone shape tensile samples (size 100mm x 6mm x 4mm) with gauge length of 32 mm were prepared as per ASTM specification and the test was done at low strain rate to maintain quasi-static condition while testing.

Chapter 4

Experimental Procedure

4.1 Work piece material

4.1.1 Dimensions

Plates of size 120 mm x 80 mm x 4 mm were shear cut from bigger plates. This shear cutting methods leave some defects like Bow, Twist and Camber in the plates which are not suitable for FSW hence prior to welding plates were ground and milled from both sides.

4.1.2 Chemical Composition

Chemical composition of both AISI-316 and Ti-6Al-4V is given in table 2 and 3.

Table 2: Chemical composition of AISI-316L.

Alloy	% C	%Mn	%Si	%Cr	%Ni	%Mo	%S	%P	%Fe
AISI-316L	0.003	2	1	16 - 18	10 -14	2-3	0.03	0.045	Balanced

Table 3: Chemical composition of Ti-6Al-4V.

Alloy	%Al	%V	%Ti
Ti-6Al-4V	6	4	Balanced

4.1.3 Mechanical properties of AISI-316 and Ti-6Al-4V

Tensile test and Vickers Hardness test were performed on base materials as per ASTM standards to obtain mechanical properties and are given in Table 4.

Table 4: Mechanical Properties of AISI-316 and Ti-6Al-4V.

Alloys	Yield strength (MPa)	Ultimate tensile strength(MPa)	% Elongation	Vickers Hardness (VHN)
AISI-316	327	608	49	190
Ti-6Al-4V	773	1118	12	320

4.2 FSW Tool

4.2.1 Tool Material

Non consumable rotating tool of hard materials is the most important requirement of the FSW process. From the literature survey, PCBN was looking as the most promising material as tool material. Megastir tool was imported from USA whose commercial name is Q70 prepared by powder metallurgy route using HPHT technology consist of 70% PCBN and 30% W and Re. W and Re metals act as matrix phase and binds PCBN together.
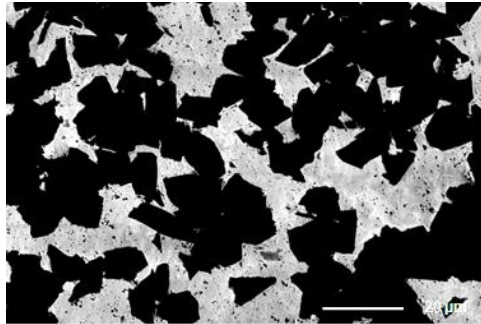
Figure 14: Q70 with W Re composite material [31]

The darker region represents Ultra-hard cBN particles finely dispersed within the metal matrix, forming a tightly bonded structure that takes advantage of both the toughness of the metal matrix and the hardness of the cBN phase. Tungsten and rhenium are relatively brittle metals with melting points in excess of 3000˚C. Alloying of rhenium in tungsten significantly improves the room temperature material toughness, this is known as the 'rhenium effect'[32]. Alloying between W and Re is evident under HPHT conditions and the alloying temperature is much lower than the temperature required for densification of W-Re alloys [33].

21

4.2.2 Tool Dimensions and Pin Profile

Tool was designed as per requirement of the FSW machine at IISc Bangalore
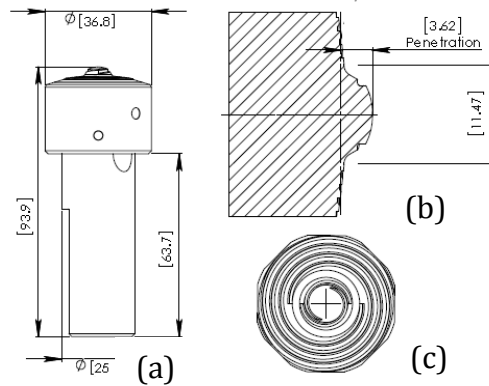
Figure 15: Schematic of Q70 Megastir tool (a) Complete tool (b) Pin (c) Top view of pin

Tool consists of two parts pin and shaft. Pin is made up of Q70 material and shaft of tungsten carbide which are coupled together by locking collar made up of high temperature material. To avoid heat flow from pin to shaft a thermal barrier is introduced in between them. The pin consists of rounded bottom with two threads and rotates in clockwise direction.

4.3 Experimental

4.3.1 Optimization of plunge depth

Plunge depth was optimized before performing actual experiments in such a way to obtain minimal flash generation and avoid damage to backing plate. Tool was plunged with a RPM of 1100 in the plate without any welding speed and plunged depth was varied every time to observe minimal flash generation. For steel 3.72mm plunge depth was optimized.

Figure 16: Photograph showing Optimization of Plunge depth for AISI-316L

For Ti-6Al-4V the plunge depth was varied in 9 experiments from 3.70 to 3.7 4mm.

4.3.2 Design of Experiments

Experiments are arranged for similar metal joining given in tables 4 and 5. For both AISI-316 and Ti-6Al-4V nine experiments were arranged by varying welding parameters RPM and Welding speed.

Table 5: Design of Experiments AISI-316L

Sr No.	RPM	Welding speed(mm/min)
T1	1100	8
T2	1100	12
T3	1100	16
T4	1000	8
T5	1000	12
T6	1000	16
T7	900	8
T8	900	12
T9	900	16

Table 6: Design of Experiments Ti-6Al-4V

Sr. no	RPM	W. S (mm/min)	Plunge Depth (mm)
W1	800	50	3.74
W2	800	70	3.74
W3	800	60	3.70
W4	600	50	3.74
W5	600	70	3.72
W6	600	60	3.70
W7	400	50	3.74
W8	400	70	3.70
W9	400	60	3.72

Plates of AISI-316 L were Friction Stir welded using ETA FSW machine at IISc Bangalore with varying RPM and Welding Speed. Tool Plunge depth and tool tilt angle were kept constant at 3.72mm and 2° for all the above shown welds. Precaution was taken to exert minimum load on tool pin. Prior to welding, plates were mechanically ground and milled from the edges. Photographs of welded plates are given in fig. 17.

Weld T1   Weld T2   Weld T3
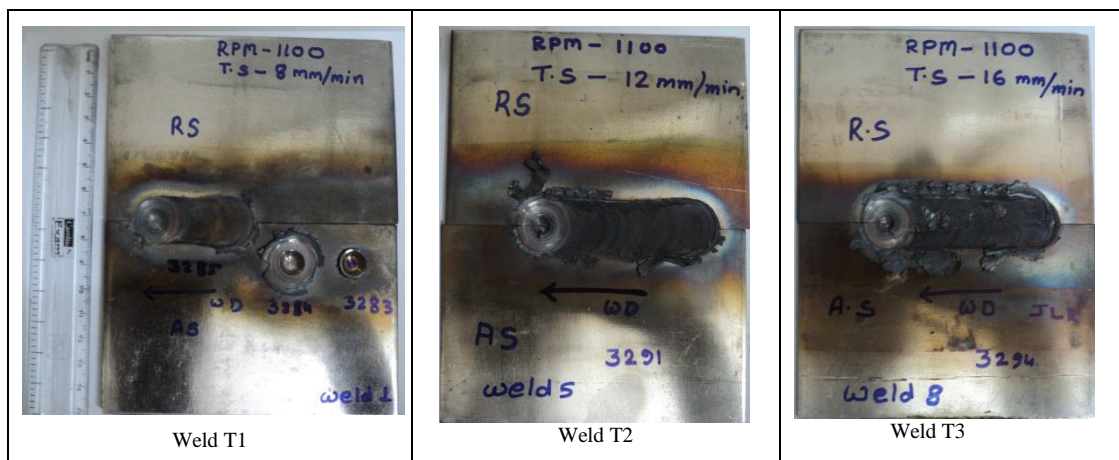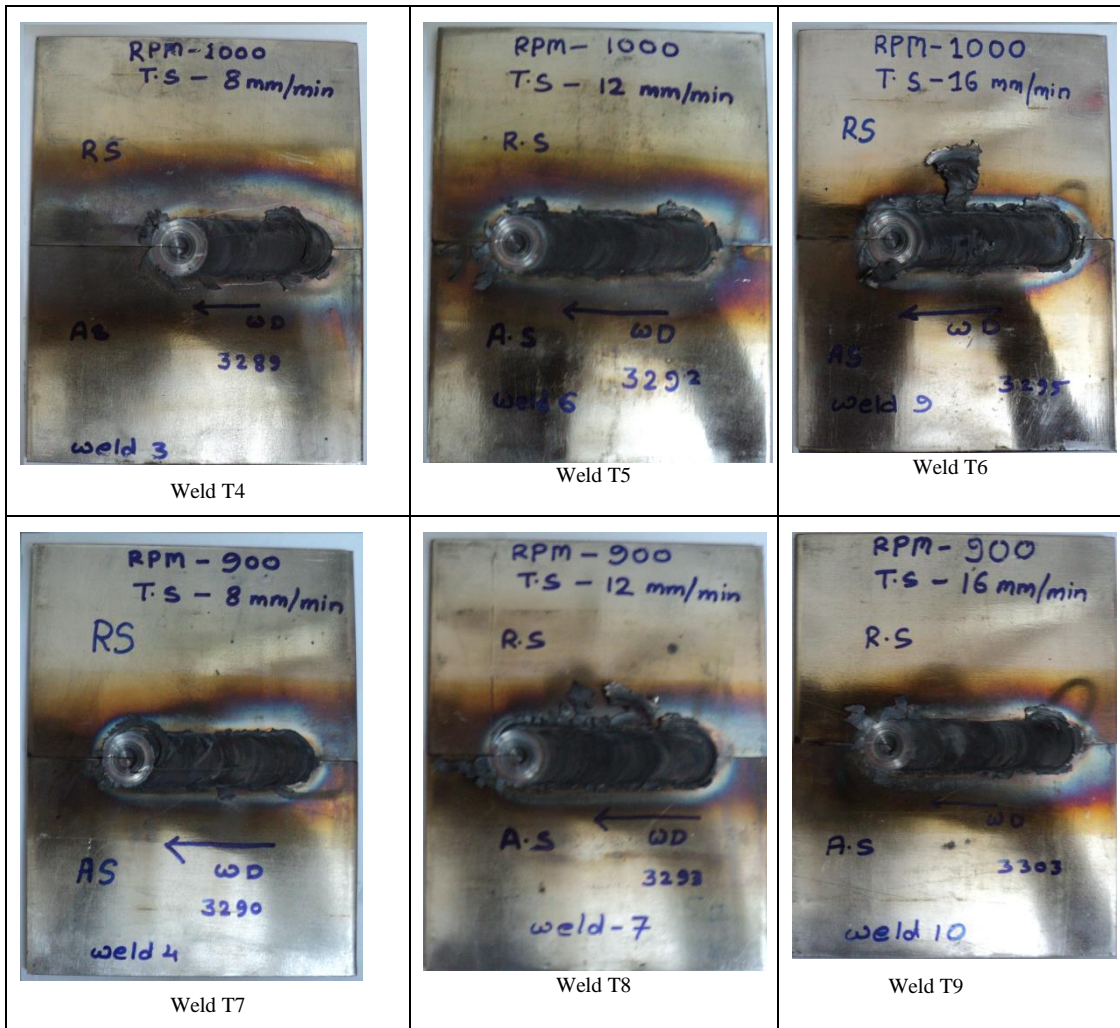
Figure 17: Photographs of Friction Stir Welded AISI-316L plates

Ti-6Al-4V plates were friction stir welded (shown in fig. 18) with constant tool tilt angle of 2°. Insufficient heat generation with weld W4 and W7 parameters plates are not welded properly as per visual inspections.
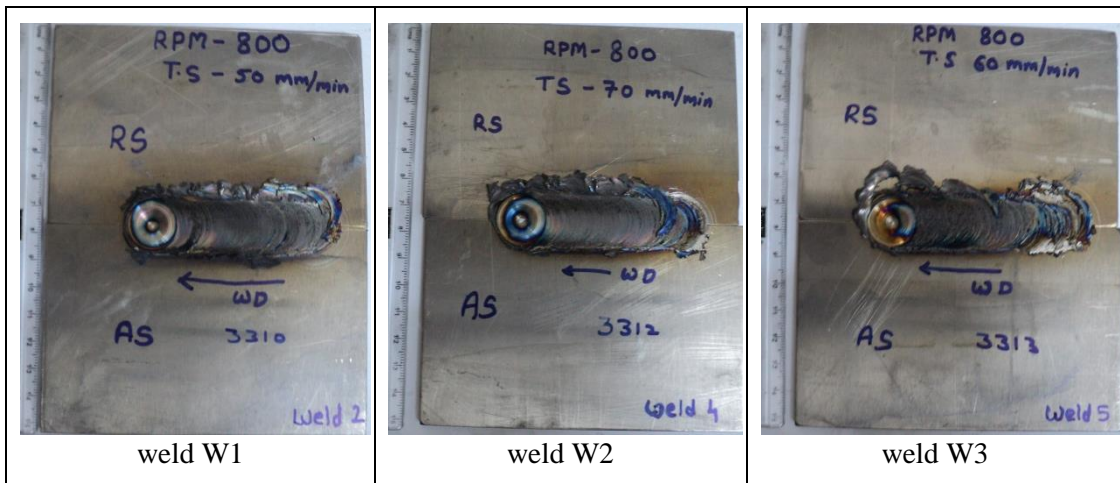
Figure 18: Photograph of Friction Stir Welded Ti-6Al-4V plates.

4.3.3 Tensile testing

Tensile samples were cut using electric discharge machine (EDM) (as shown in Figure 19) to evaluate transverse tensile properties and tested with a strain rate of $10^{-3}s^{-1}$ as per the guide lines of ASTM E8M specification.
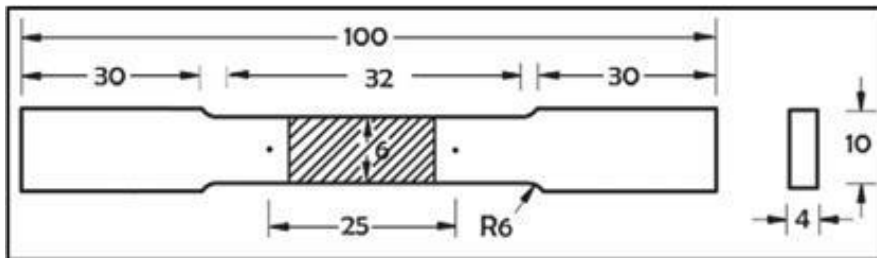
Figure 19: Tensile Specimen of E8M specification (Dimensions in mm).

4.3.4 Vickers Hardness testing

Hardness profile was taken at regular interval of 1 mm on the cross section perpendicular to the welding direction of all the welds. For AISI-316L 0.98N of load was used with a dwell time of 15 seconds to get the hardness profile while for Ti-6Al-4V load of 4.9N was used with a dwell time of 10 seconds.
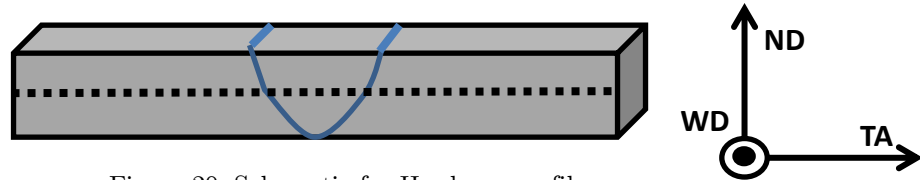
Figure 20: Schematic for Hardness profile

4.3.5 Optical Microscopy

The specimens for OM were cut perpendicular to the welding direction by EDM and were mechanically ground with silicon carbide grinding paper (180, 600, 1000, 1500, 2000 grit) and diamond suspension (9, 6, 3 and 1 µm), followed by electropolishing with A3 solution (10% perchloric acid + 30% methanol + 60% butanol). AISI-316l was etched in methanolic aqua regia and Ti-6Al-4V with Krolls etchant for 20 s. Krolls reagent is mostly a low contrast etchant reveals general microstructure of α-β alloys.

 4.3.6 Scanning Electron Microscopy

For SEM analysis sample was prepared the same as for OM. 6 to 7 Kikuchi bands were used for indexing each pattern to minimize the possibilities of misindexing error. Step size and magnification were maintained as 4µm and 100X for AISI-316L and for Ti-6AL-4V 1µm and 400X respectively to acquire whole map while the hit rate was varying from 60 to 90%. Grain dilation was used as cleanup type with parameters grain tolerance angle 5, minimum grain size 2 and single iteration. To define low angle grain boundaries (LAGBs) 2° to 15° misorientation angle criteria of rotation angle while for high angle grain boundaries (HAGBs) 15° to 180° was used. All EBSD micrographs were taken in the TA–ND plane and are presented such that the TA was horizontal and the ND was vertical. The acquired EBSD data was

analyzed using HKL and TSL-OIM™ analysis software to plot Pole Figure, Inverse Pole Figure, Grain size Measurement and its Distribution, Misorientation Profiles and Grain Boundary analysis.

Chapter 5

Results

5.1 Observation in variation of Torque and forces during experiments of AISI-316L

Description of axial loads, torque and tool position against time is given in figure 21. Total cycle time is of 317 seconds.

Stage 1- Initial 27s was taken by tool to reach plunge depth of 3.72mm. During plunging (0-27s), the axial load rose initially when the pin was in contact with the cold workpiece and quickly fell as the material was softened due to heating. The softened material was displaced until the pin again encountered colder material, and the process then repeated. But with increasing depth, the friction at the circumference of the pin has also an effect on the axial load and on the torque. The temporary drop at 20 s could be due to localized melting in the region below the tool. Initial load curves exhibited several "spikes" up to 12 kN during the first 27 s of the plunging period prior to welding. The spike in load up to 15 kN occurring at approximately 30 s corresponded to the point in time when the shoulder contacted the top surface of the plate.

Stage 2- For next 45s the material below tool was simultaneously heated and deformed leads to plasticizing of material as a result Z-axis load decreases from 15kN to 8kN. Spikes in Z-axis load arises as cold material comes in contact with tool.
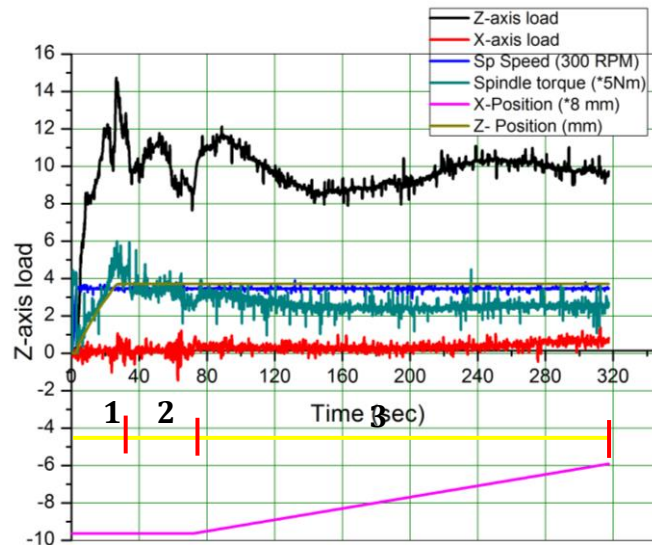
Figure 21: Welding Forces Vs Time graph

Stage 3 – Further from 75s of the cycle tool starts traversing in welding direction, Z- axis load reaches to 12 kN as cold material comes in contact with tool. During traversing of the tool Z-axis load curve decreases smoothly from 12kN to 8kN (75s to 160s) and further rose to 10kN (220s) then remains steady till the end of cycle.

5.2 Optical Microscopy

5.2.1 Optical Microscopy of AISI-316L

The optical micrograph of the transverse section of the base material is given in fig 22. The base material was obtained as heat treated rolled sheet and consists of equiaxed austenite grains containing several annealing twins.
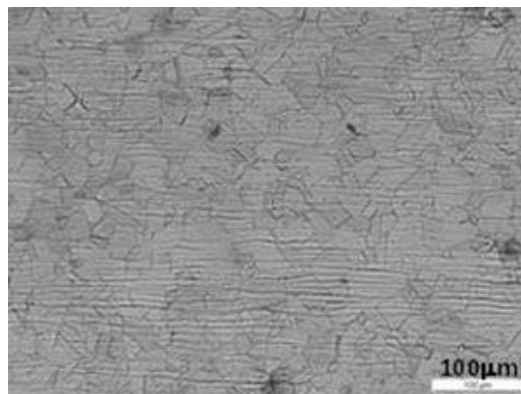
Figure 22: Optical image of Base Material AISI-316

Optical micrographs of transverse section of the welded specimens are shown in Fig. 23. The weld specimens in the transverse section showed mainly the central nugget

29

zone followed by TMAZ, HAZ and then base material. The grains appeared equiaxed and smaller in the nugget zone than in the base material.
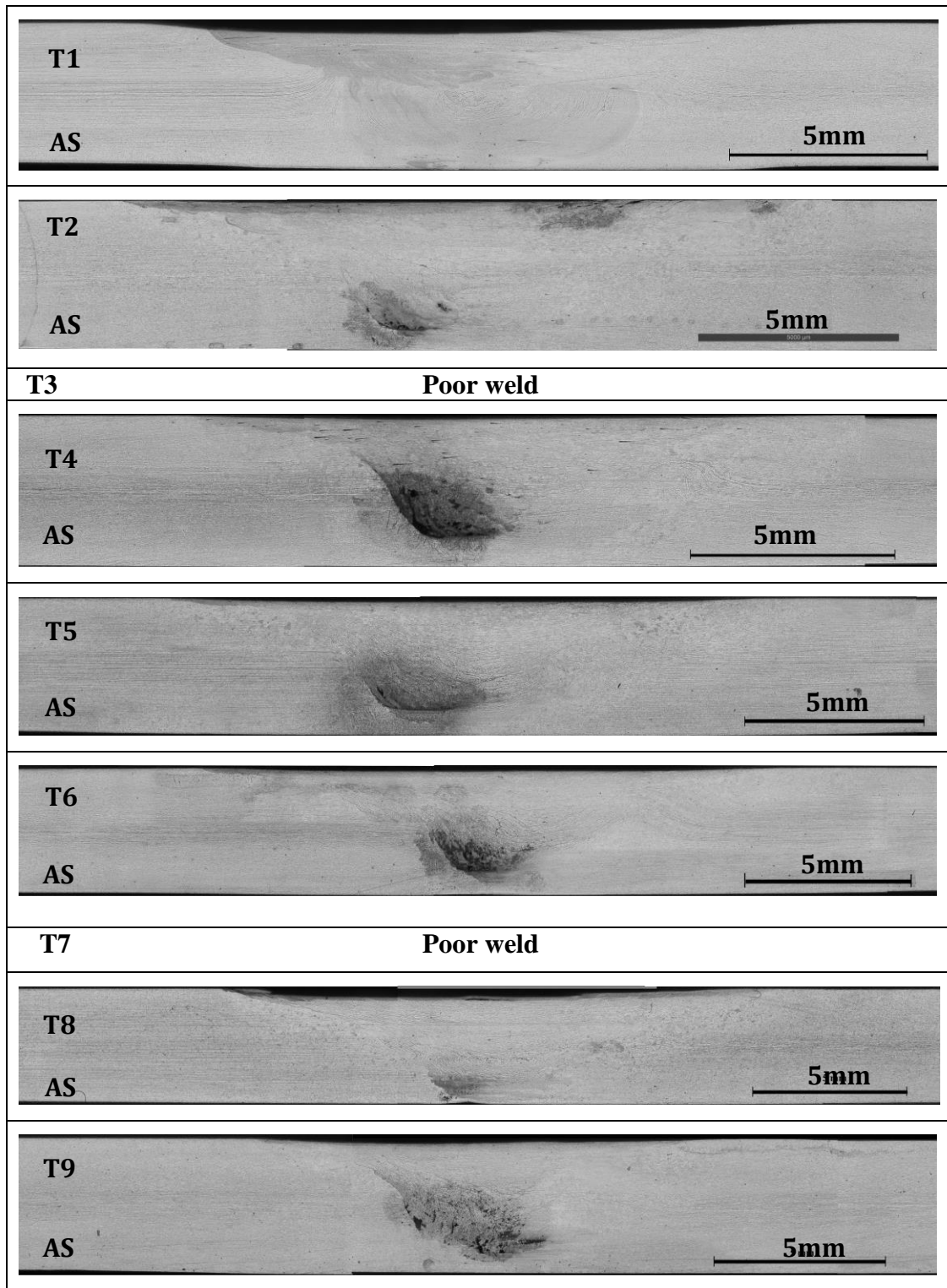
Figure 23: Optical micrographs showing transverse sections of AISI-316L welded samples (AS denotes advancing side). T7 is not shown as it was a poor weld.

In all the welds, a clear contrast appeared at around 3-4 mm from the center of the nugget zone between TMAZ and nugget region in the advancing side, stating not proper mixing. The contrast is appeared less in the retreating side. Inside the nugget zone, the material flow lines represent the material being swayed from the advancing side and mixed forcibly into the retreating side, creating smooth transition with no contrast. Except T1 weld, the rest of the welds contain several defects like pores at the bottom of the nugget zone region.
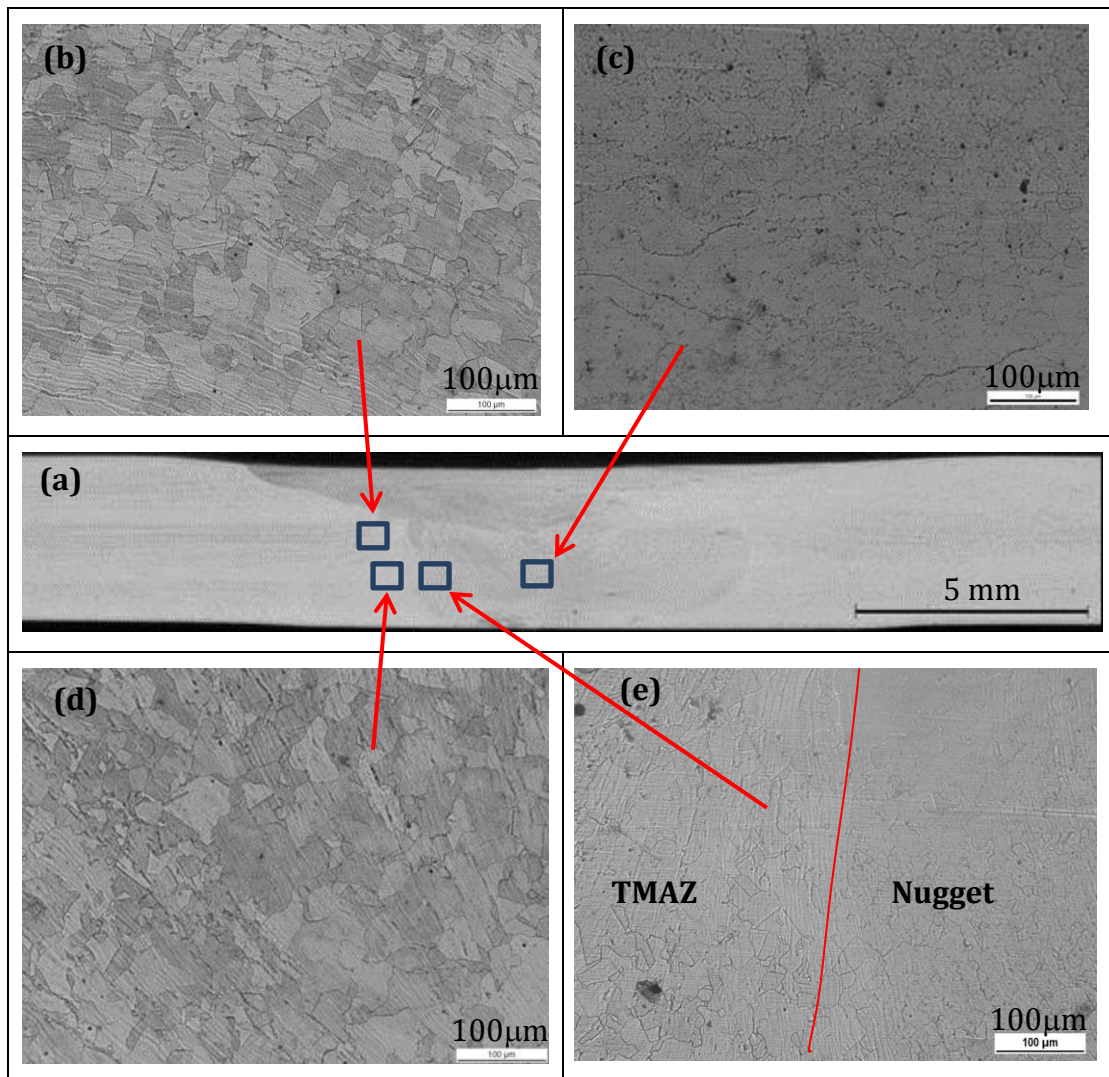
Figure 24: Various zones in T1 weld (a) Macrostructure of transverse section (b) HAZ (c) Nugget Zone (d) TMAZ (e) Nugget + TMAZ

T1 weld with bottom part containing onion rings like microstructure is given in fig 24. The optical images at various weld zones (SZ, TMAZ, HAZ) of sample T1 are shown in fig 24. Due to stirring action of tool, the grains in the nugget zone are

with no twin boundaries as were present in the base material. This can be attributed to the thermal and mechanical actions experienced by this material, which caused shear and may be further dynamic recrystallization. Grains in TMAZ and HAZ seem to be larger than the base material and nugget zone. In figure 24c deeply etched lines along grain boundaries can be observed in nugget zone.

5.2.2 Optical Microscopy of Ti-6Al-4V

The optical micrograph of the transverse section of the base alloy is given in Figure 25. It consists of deformed α (hcp) and β (bcc) grains. Elongated α grains in matrix of β phase in one direction suggests cold rolled or warm rolled microstructure of base material.
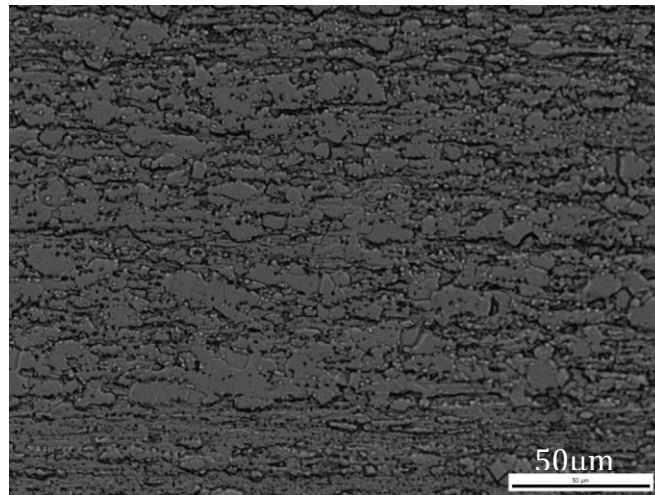
Figure 25: Optical image of Base material Ti-6Al-4V

Macrostructure of transverse section of the welds are given in fig 26 showing clearly the nugget zone. To reveal other zones in weld, further microscopic analyses are performed at high magnification.
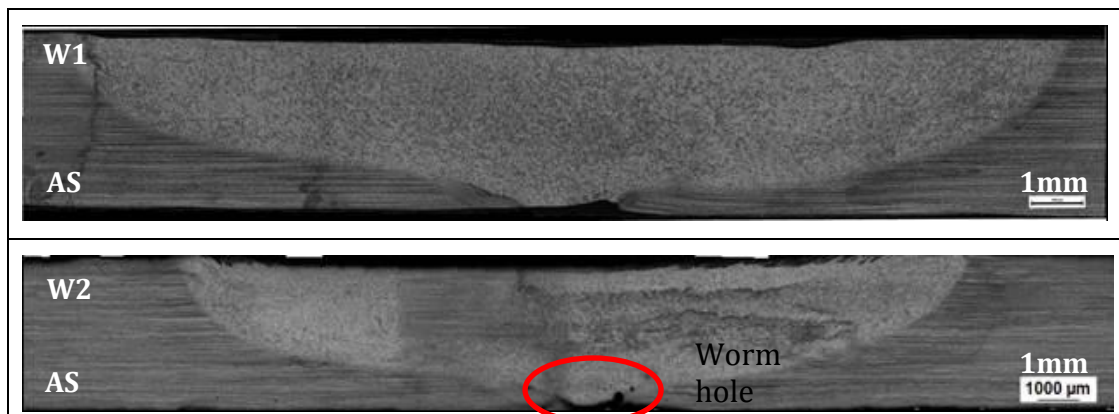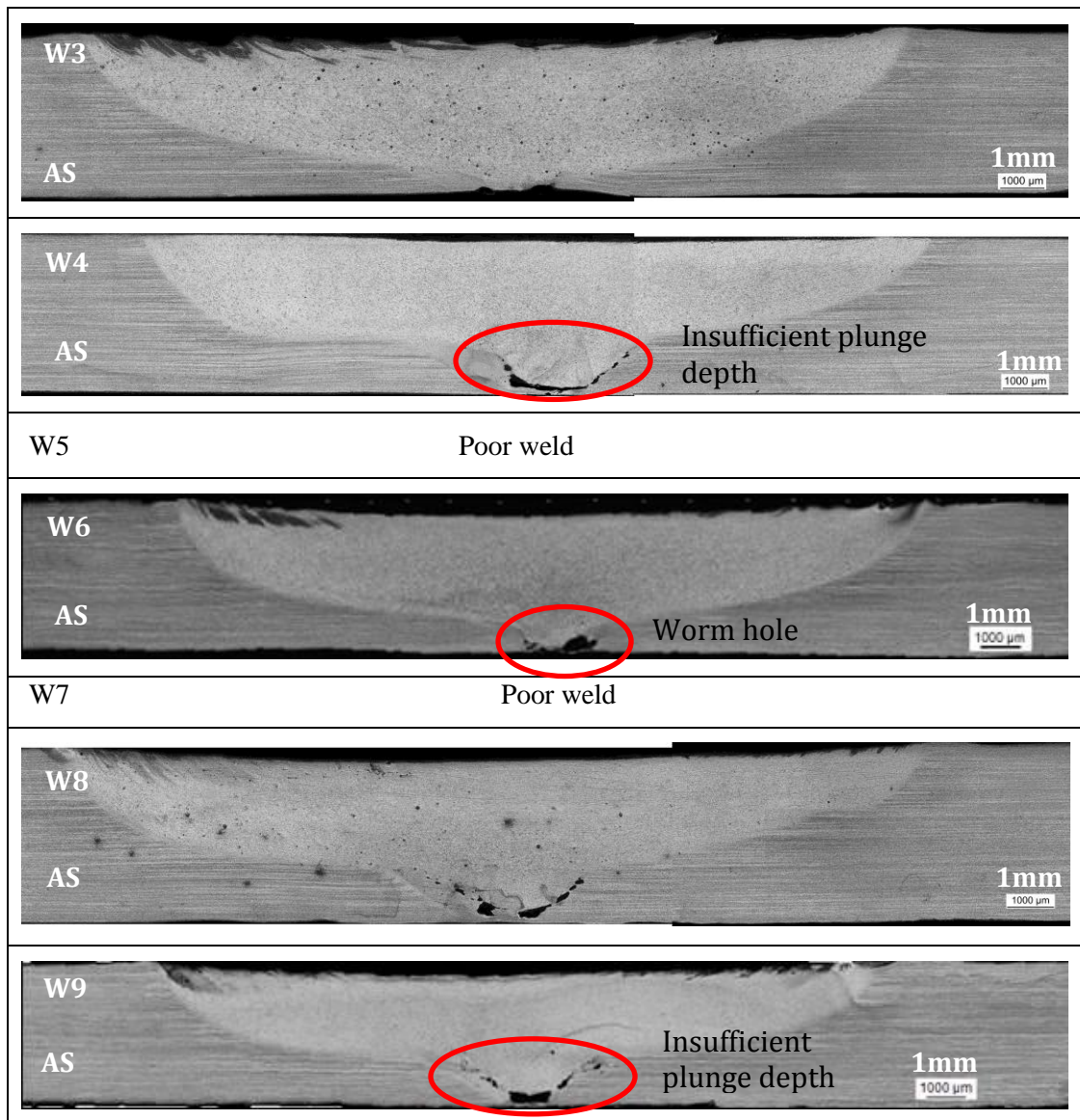
Figure 26: Macrostructure showing transverse section of Ti-6Al-4V welded sample. W5 and W7 were of poor weld and not shown here.

Except in welds W1 and W3, various defects like worm holes and incomplete root penetration are observed at the bottom of weld nugget. These defects are seen in welds of high welding speed with lower rotations. The noticed worm holes in W2 and W6 are might be from high welding speed while in W4, W8, W9 having incomplete root penetration (shown in Fig 26) is observed due to low plunge depth. No worm holes and root penetration defects were noticed in W1 and W3 welds.

Figure 27 shows micrographs corresponding to four different zones of W1 weld. The central weld part (nugget zone) in Figure 27a and 27b showed fine lamellar

Widmanstätten secondary α laths in the matrix β phase grains, stating their reaching the high temperature single β phase region during stirring followed by generation of Widmanstätten secondary α laths during cooling. Whereas, the thermomechanically affected zone (Fig.27d) in the advancing side showed bimodal (equiaxed primary α grains + secondary β laths) microstructure. This indicates the thermomechanical processing in the α+β region only.
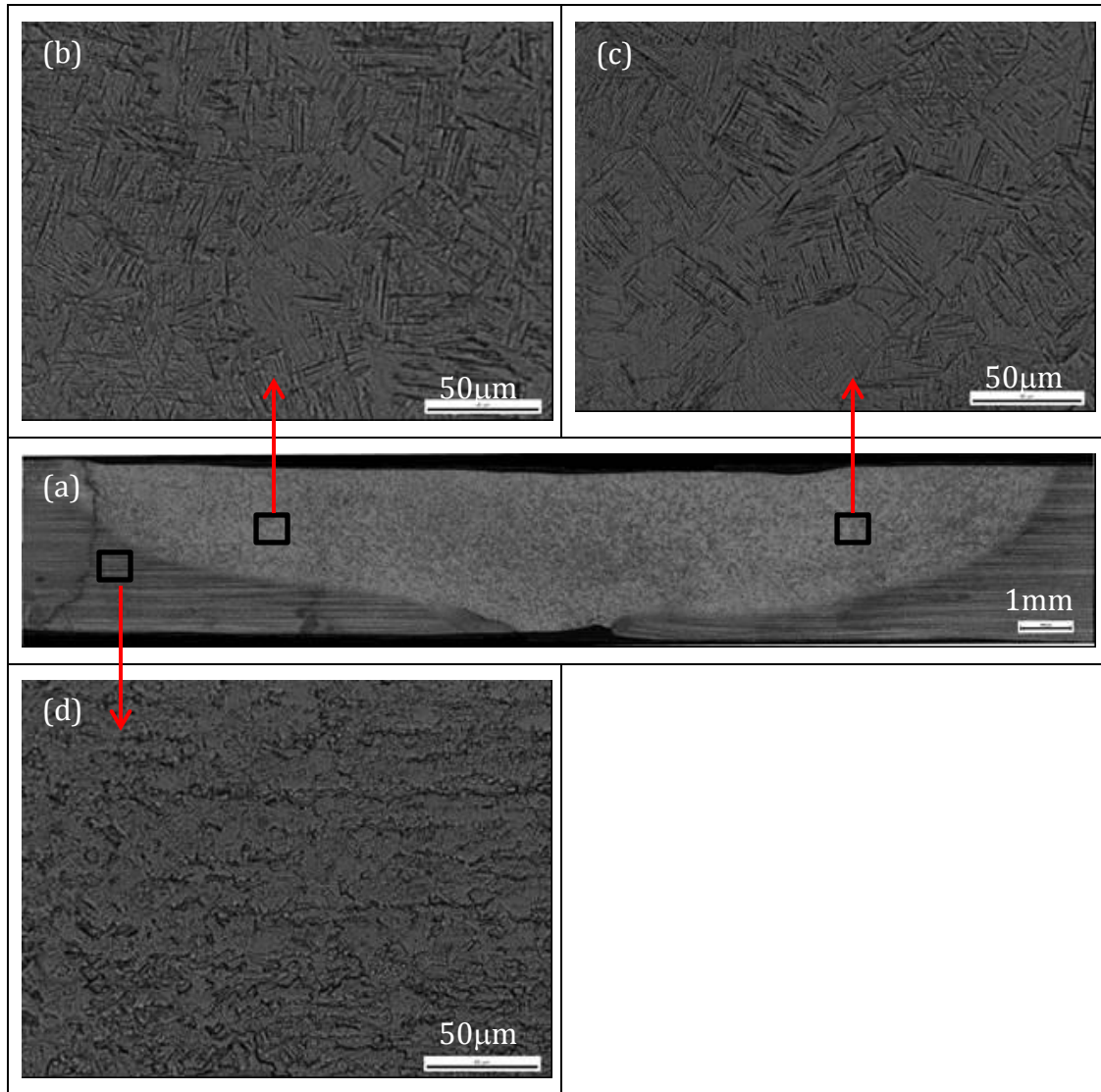
Figure 27: Different zones in W1 weld (a) Macroscopic transverse section (b) Nugget zone (AS) (c) Nugget zone (RS) (d) TMAZ

5.3 Vickers Hardness

5.3.1 Vickers Hardness of AISI-316L
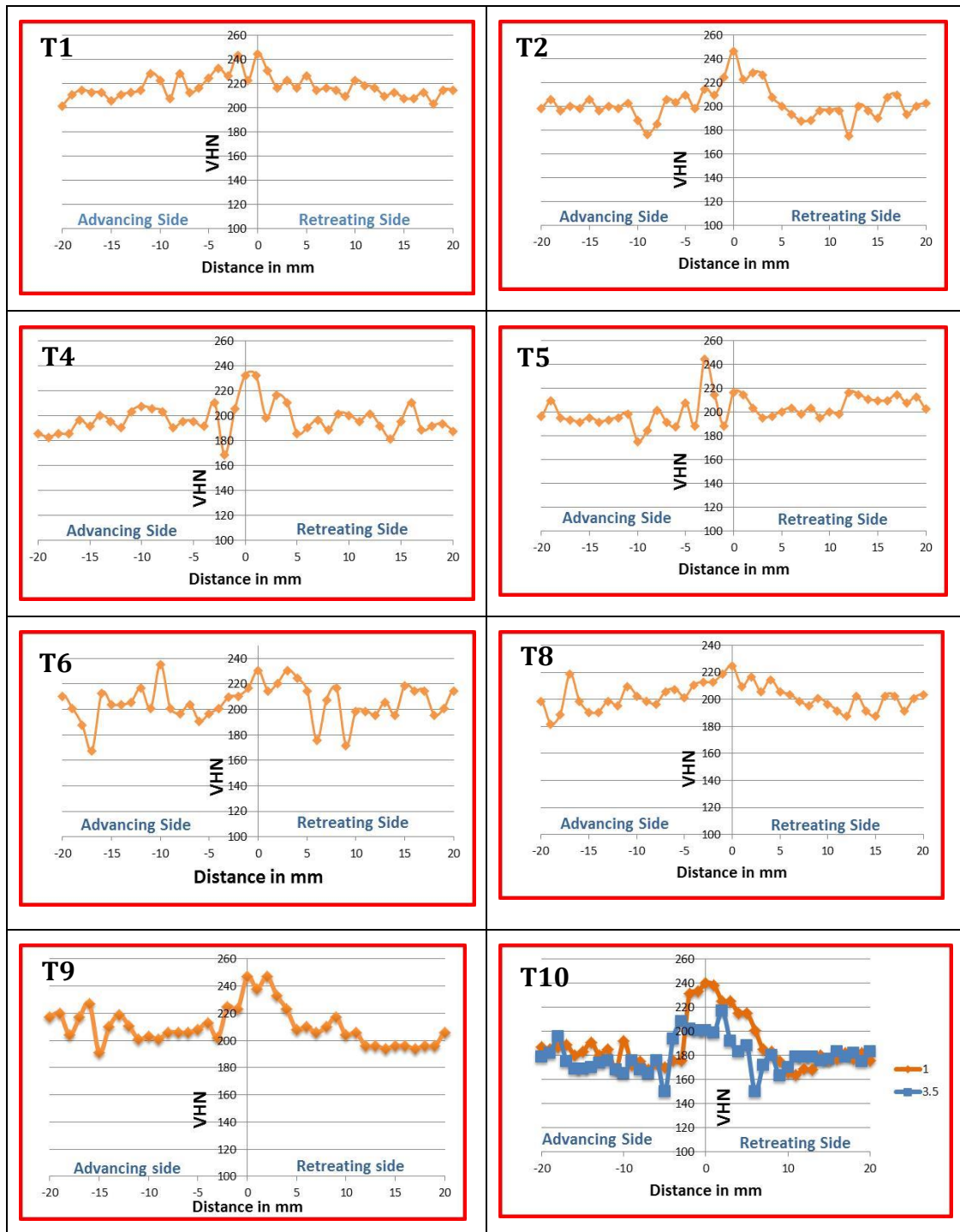
Figure 28: Vickers hardness profile of AISI-316L welds (T1 to T9) (T10 w.r.t weld depth in T1 weld)

Vickers hardness tests were performed on the cross section perpendicular to the welding direction of the base material. The hardness value of 190 VHN is obtained for the base material. The hardness profiles of all welds are given in fig 28. T1 to T9 represent profile from middle and T10 shows variation in profile w.r.t depth of weld in T1(top and bottom). The indentation was taken after every 1mm to detect the changes in hardness at various zones. In the center of all the welds, a rise in hardness was observed. This is due to the stir generated finer grains in the nugget. Also in the stir zone region of T1 weld, higher hardness at the top of the bead is observed (fig 28 T10) due to the presence of fine grain structure which arises due to severe thermomechanical deformation of that area by touching of the tool shoulder. The hardness goes on decreasing as the shoulder effect decreases in the nugget zone.

5.3.2 Hardness profile for Ti-6Al-4V
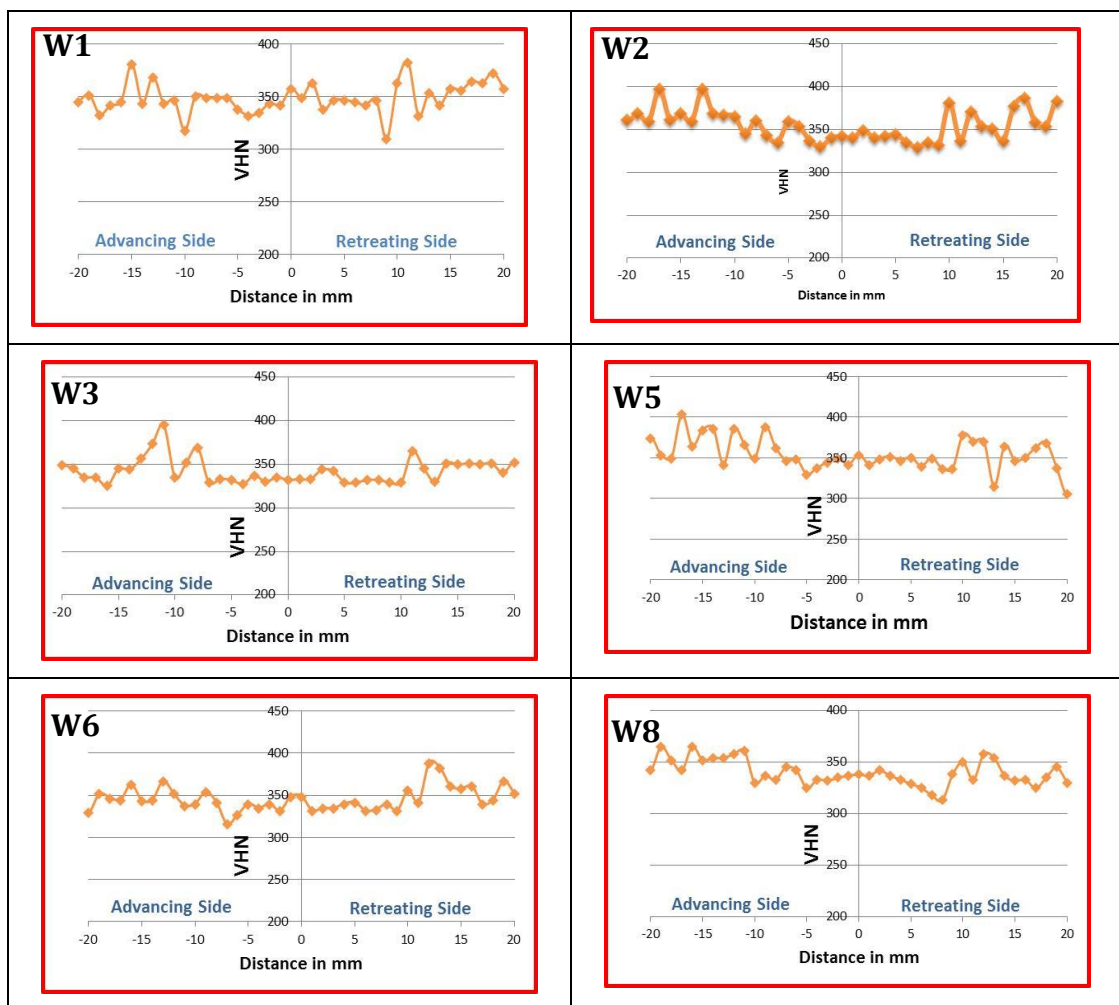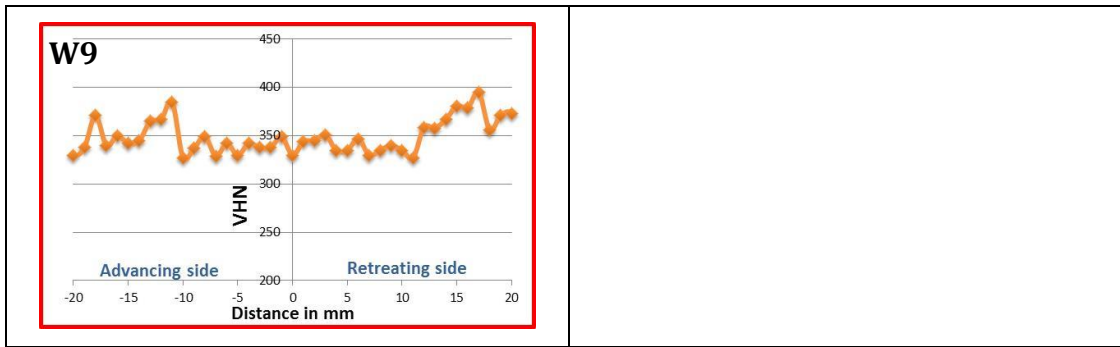
Figure 29: Vickers hardness profile of Ti-6Al-4V welds.

The hardness profiles from advancing side to the retreating side of all welds are given in fig 29. The average base material hardness is 330 VHN. There noticed variation in hardness values in the base material region which is due to the presence of hard and soft α and β grains with less deviations towards the nugget zone containing α laths in β matrix grains only

5.4 Tensile test

5.4.1 Tensile tests of AISI-316L welds
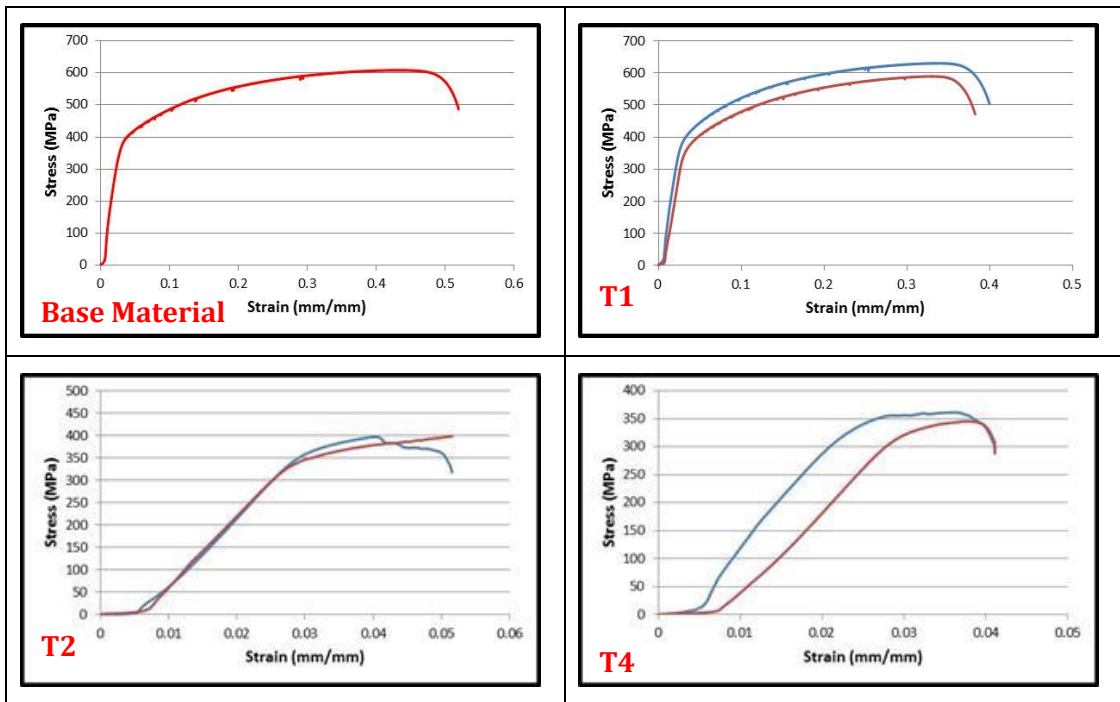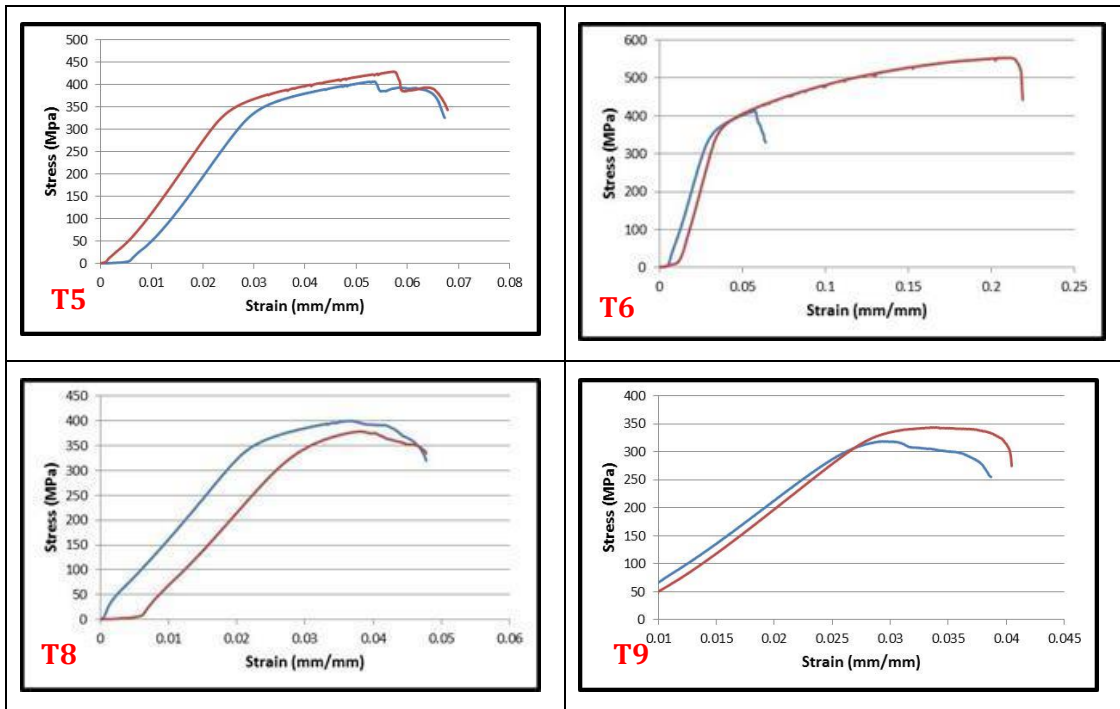
Figure 30: Tensile test plots for AISI-316L welds

Tensile tests (two on each weld) were performed on the base material and the welded samples and the results obtained were compared with the base material. The results are given in table 6 and their graphical plots are shown in fig 30. Excellent average 610 MPa UTS value is obtained from the T1 weld, which is just above the base material (608 MPa), with an average elongation of 35% (elongation of 49% in base material).

Table 7: Tensile Results of AISI-316L welds.

Sr. No	RPM	Welding Speed (mm/min)	UTS (MPa)			% Elongation		
			1	2	Average	1	2	Average
T1	1100	8	630	590	610	37	32	35
T2	1100	12	397	345	371	5	1	3
T3	1100	16	-	-	-	-	-	-
T4	1000	8	361	443	402	3	7	5
T5	1000	12	428	407	417	5	3	4
T6	1000	16	553	378	465	20	2	11
T7	900	8	-	-	-	-	-	-
T8	900	12	399	412	405	5	2	3.5
T9	900	16	343	318	330	5	1	3
Base Material			608			49		
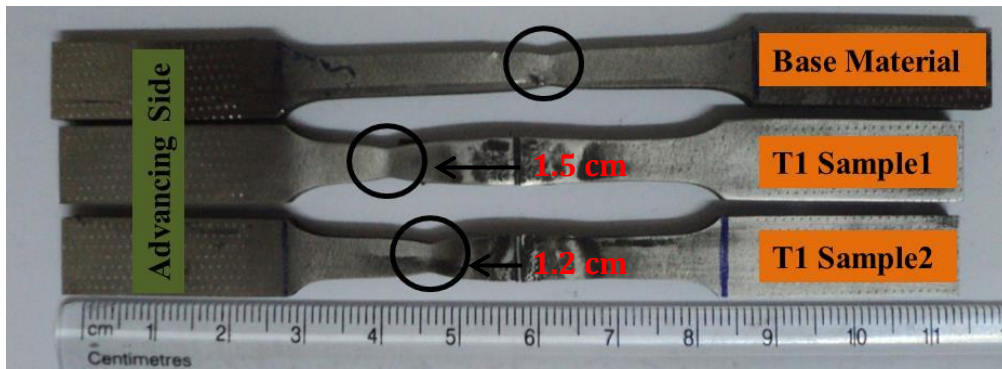
Figure 31: Photograph of tensile samples after test showing necking.

T1 weld showed necking at around 1.5 cm away from center at the advancing side of the base material region as shown in fig 31. Except T1, the rest of the welds necked and fractured in the advancing side in between 3-4 mm from the nugget zone (at the nugget zone–TMAZ interface). This is expected with the fact of sudden change in grain microstructure between the nugget zone and the TMAZ, hence becoming the weak region and therefore, failed first under stress. Containing no defects (pores) and relatively smooth transition of the grain structure from the nugget zone to the TMAZ and then to the base material, the weld region of T1 (shown in optical images) under stress behaved quite similar like the base material and hence, achieved base material equivalent UTS value. Similar values of plastic yield and work hardening behavior in the plastic region between the T1 weld and the base material, suggesting achieving of a good welding condition for this austenitic stainless steel.

5.4.2 Tensile tests of Ti-6Al-4V welds
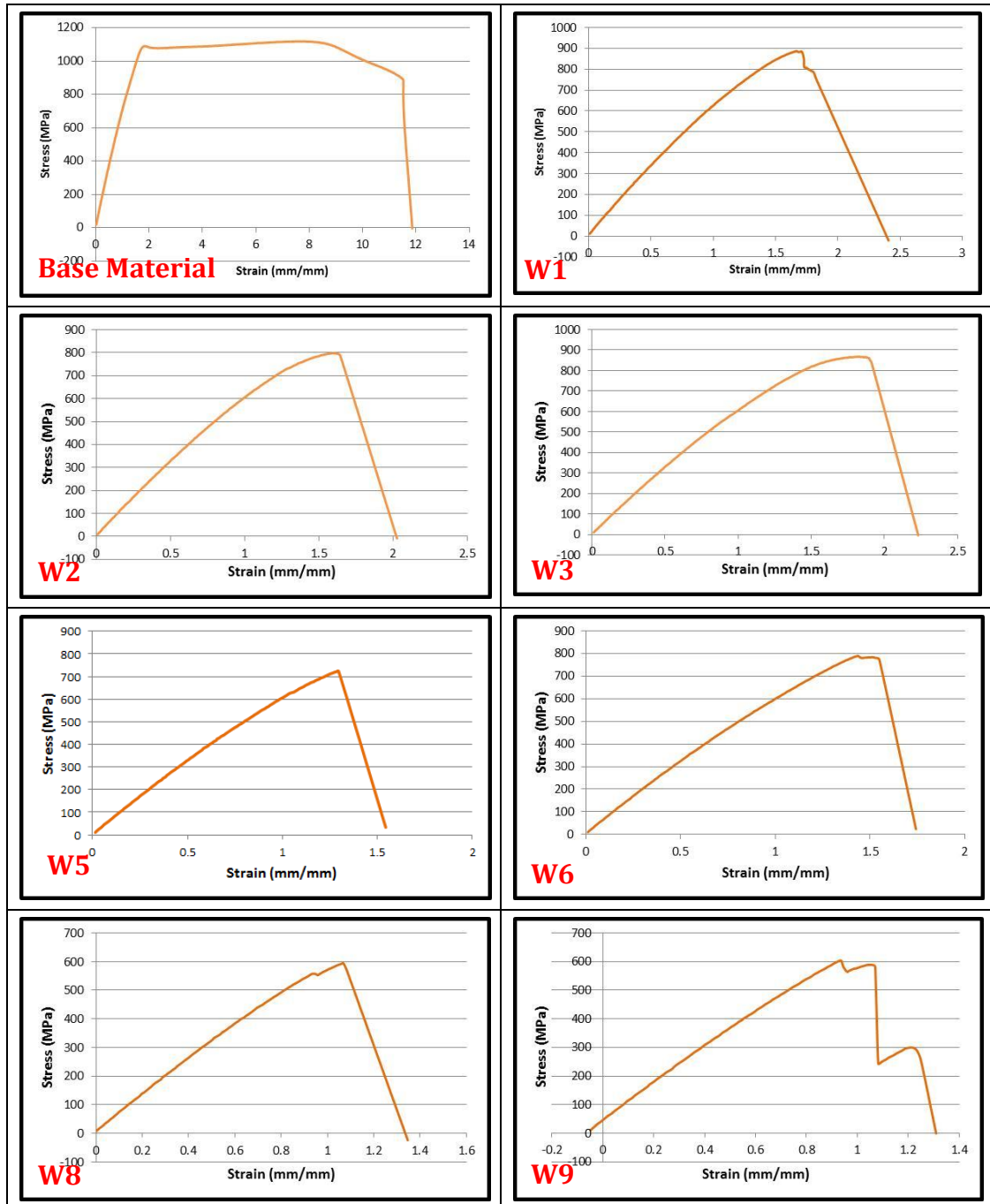
Figure 32: Tensile test plots for Ti-6Al-4V welds

Tensile tests were performed on the welded samples and the results obtained were compared with the base material. The results are shown in table7 and the graphical plots are given in figure 32. All the welds necked and fractured in the nugget zone where fine lamellar Widmanstätten secondary α laths in the matrix β phase grains

40

are observed due to transformation from high β transus temperature. Weld 1 and weld 3 have shown around 75% of weld strength as compared to base material with minimal elongation of 2 %. This clearly shows non-feasible welding of Ti-6Al-4V with Q70 Megastir tool.

Table 8: Tensile Results of Ti-6Al-4V welds.

Sr. No	RPM	Welding Speed (mm/min)	0.2 % proof stress (MPa)	UTS (MPa)	% Elongation
W1	800	50	672	887	1.8
W2	800	70	616	700	1.4
W3	800	60	680	867	1.9
W4	600	50	-	-	-
W5	600	70	641	723	1.3
W6	600	60	605	789	1.5
W7	400	50	-	-	-
W8	400	70	510	615	1.1
W9	400	60	556	593	1
Base Material			773	1118	12

5.5 Orientation Image Microscopy

Scanning electron microscopy (SEM) is used for crystallographic characterization of materials mainly to measure orientation of grains, varieties of grain boundaries, etc. Electron backscattered diffraction (EBSD) is used to collect this data. Orientation maps and pole figures are generated from these obtained EBSD data.

5.5.1 Orientation Map of AISI-316L Weld

Figure 33 represents orientation map of weld T1 taken from center of the stir zone to base material in advancing side. Attempting to obtain a deeper insight into the material flow and microstructural evolution, EBSD maps are obtained from the location shown in Fig 33 where individual grains are colored according to their crystallographic orientations relative to the [010] || TA direction (an orientation code triangle is given in figure). Multiple maps are taken and then stitched properly to show various zones in single map. Region 1 to 4 belongs to stir zone while region 5 and 6 represent heat affected zone (HAZ) and base material respectively.
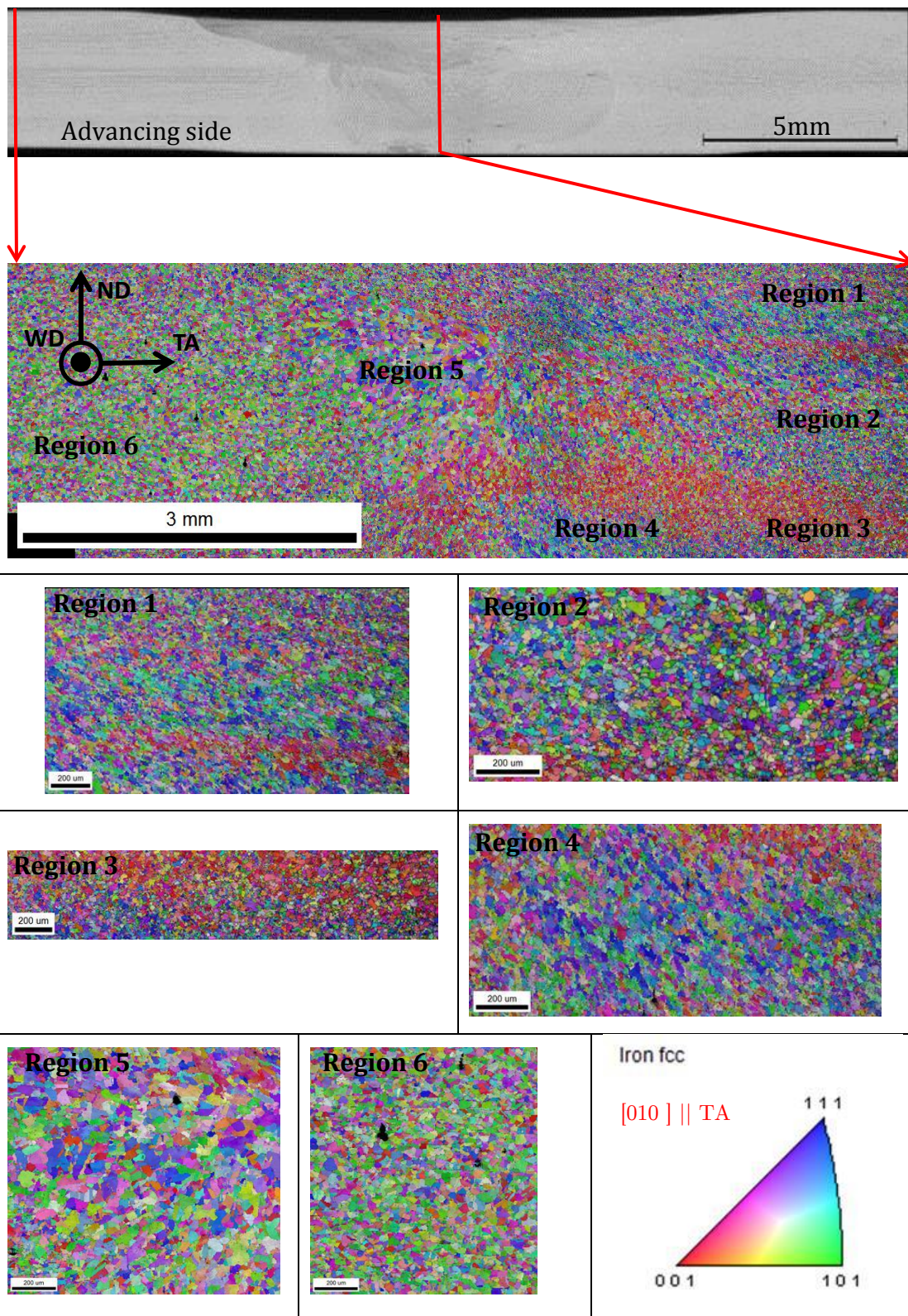
Figure 33: IPF Map [010] || TA of weld T1 showing various zones.

5.5.2 Orientation Map of Ti-6Al-4V Weld

Figure 34 represents orientation map of weld W1 taken from center of stir zone to base material in advancing side. To obtain more understanding of the material flow and microstructural evolution, EBSD maps were taken from the location shown in Fig.34 where individual grains are colored according to their crystallographic orientations relative to the [010] || TA direction (an orientation code triangle is given in figure). Multiple maps are taken and then stitched properly to show various zones in single map. 34(a) belongs to the base material while (b) and (c) show the TMAZ and the stir zone respectively.

(a) Base material   (b)TMAZ   (c) Stir Zone
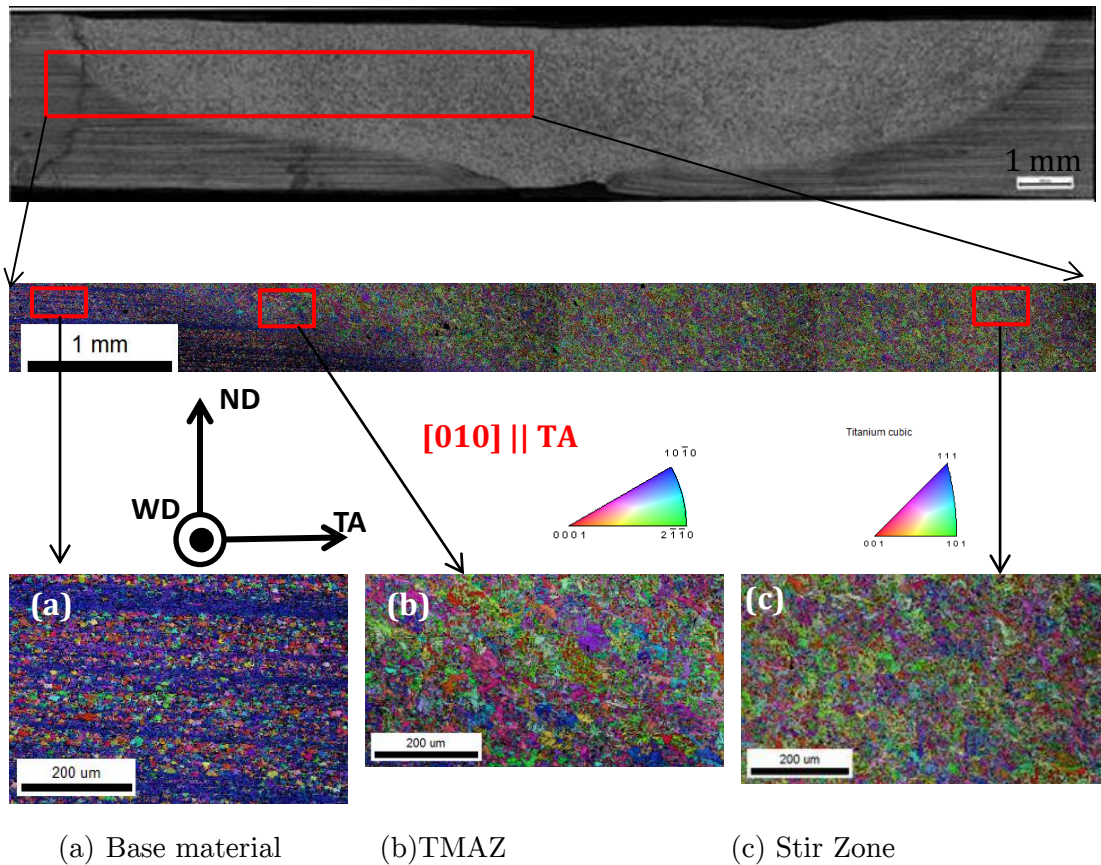
Figure 34: IPF [010] || TA Map of weld W1 showing various zones.

43

5.6 Texture Analyses

5.6.1 Texture Analyses of AISI-316L

Austenitic stainless steel (AISI-316L) is alow stacking fault energy (SFE) alloy with low dislocation mobility which prevents dislocation rearrangement into sub-boundaries and gives rise to high dislocation density. Low SFE enables deformation twinning and heavy shear band formation.

5.6.1.1   Pole Figures

The placement of the crystal plane poles of the polycrystalline grains in the specimen coordinate system is called pole figure (PF).
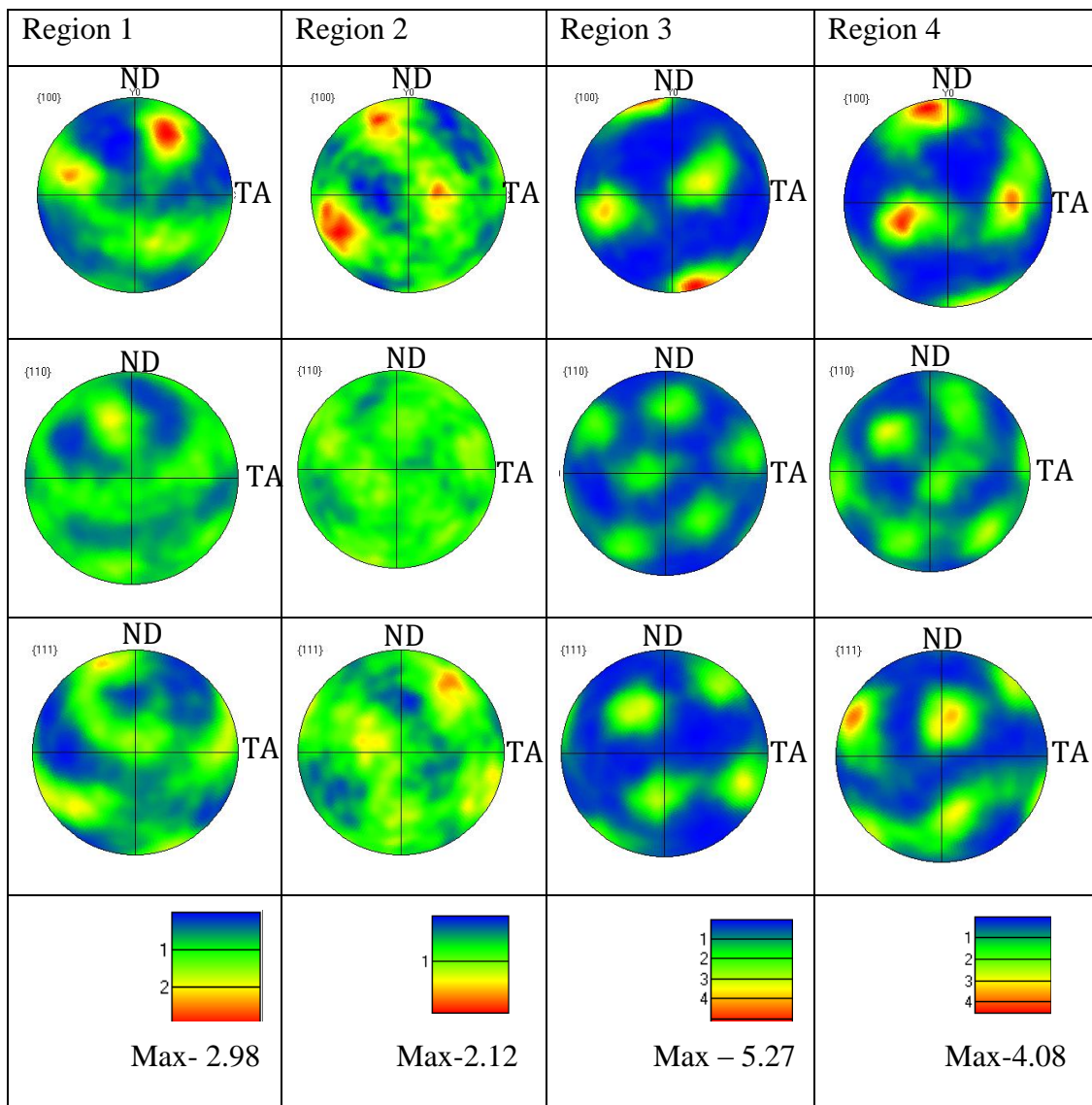
Figure 35: Pole Figure of various regions of stir zone in weld T1.

Region 5 (HAZ)	Region 6 (Base Material)
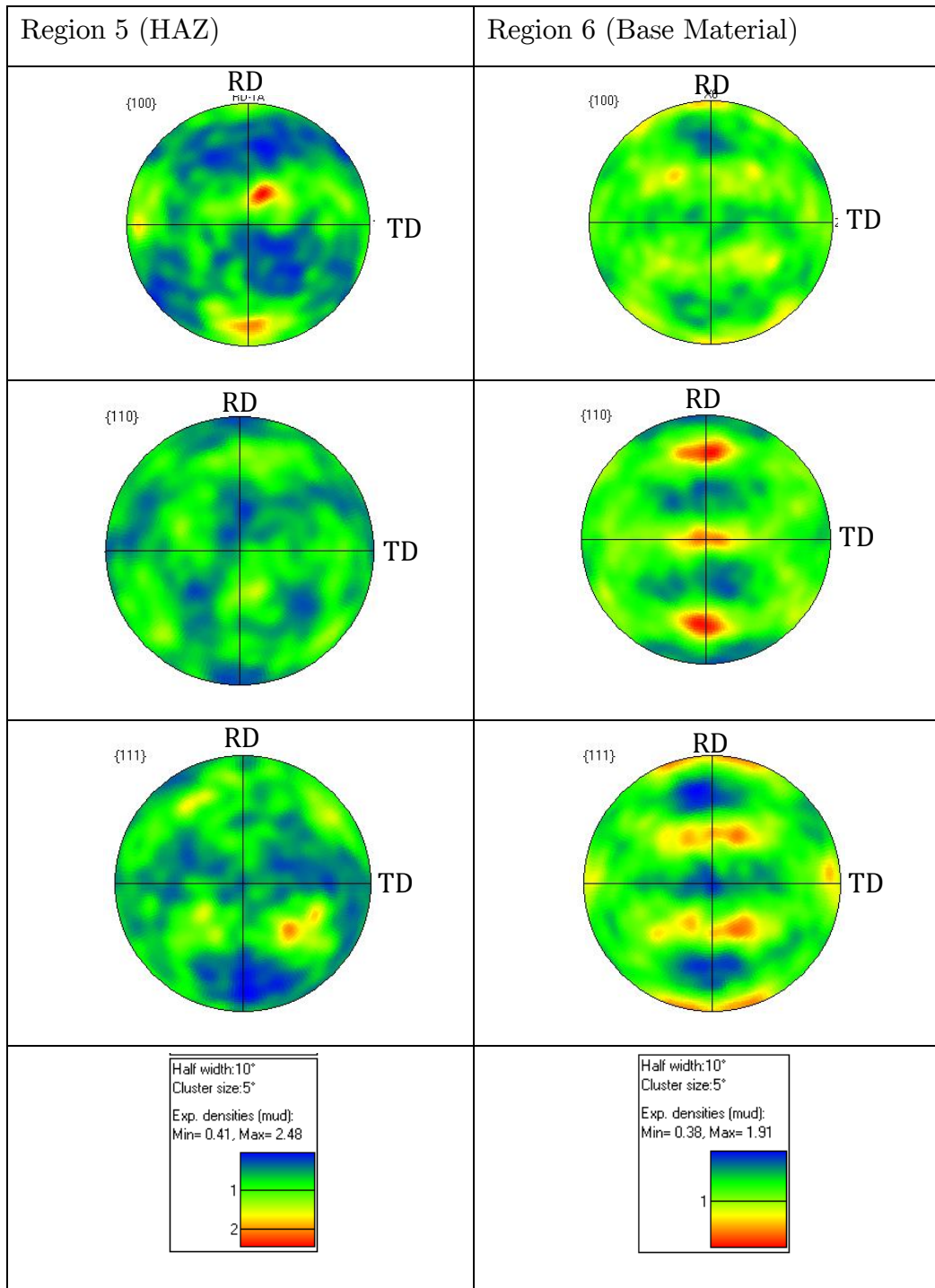
Figure 36: Pole Figure of HAZ and base material

To evaluate texture of various zones of the weld T1, the stitched EBSD map was divided in 6 regions. The characteristic 100, 110 and 111 pole figures representing

45

the preferential crystallographic orientations in these regions are given in Fig. 34. The pole figures have the reference directions ND as vertical and TA as horizontal for Stir zone and RD as vertical and TD as horizontal for HAZ and BM as in fig 35.

5.6.1.2 Grain Boundary Analyses
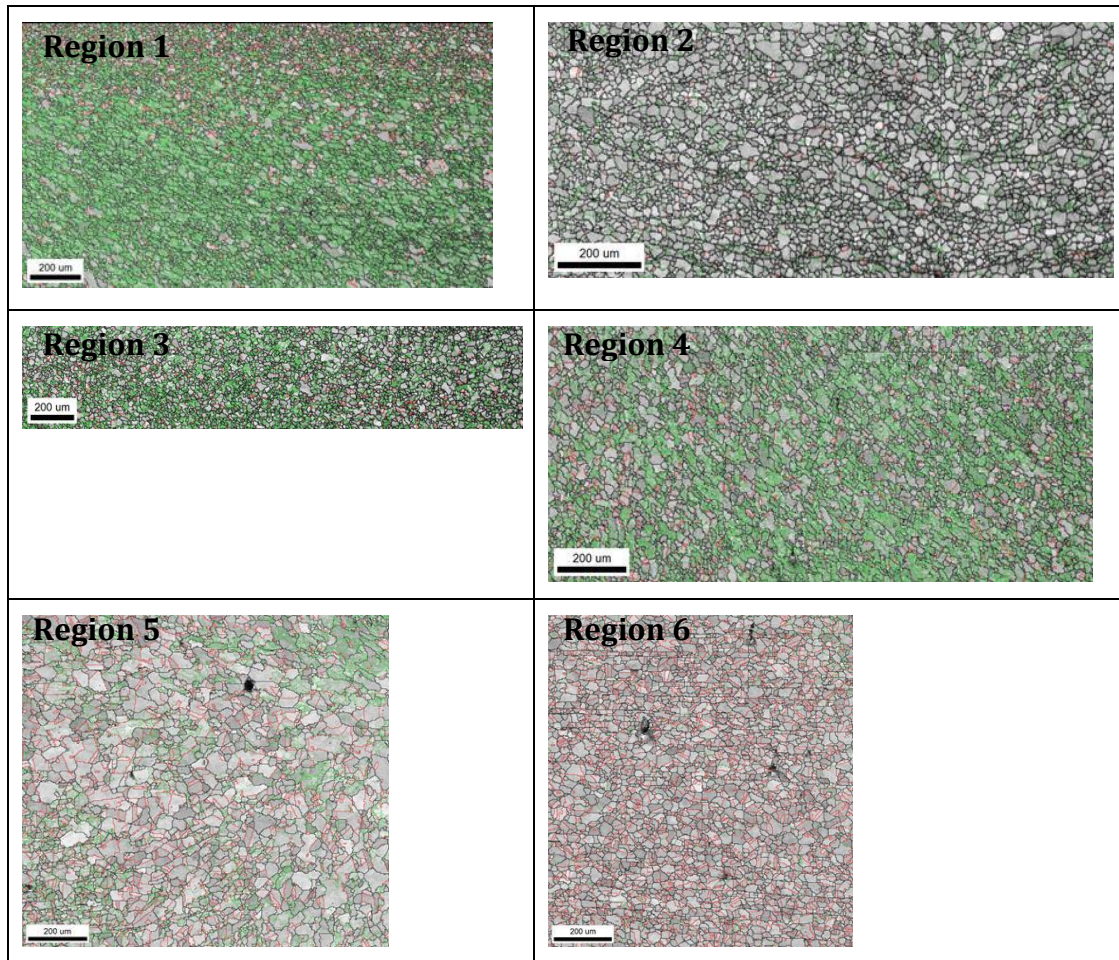
Figure 37: Grain-boundary maps showing microstructures in different regions. In the maps, LAGBs, HAGBs and Σ3 twin boundaries are depicted as Green, black and red lines, respectively.

In the EBSD maps shown in fig 36 LAGBs are depicted as thin green lines, HAGBs as solid black lines and ∑3 twin boundaries as solid red lines. Total boundary length in the map is divided into HAGBs and LAGBs which gives satisfactory explanation of mechanism behind microstructural evolution. Within stir zone grain boundaries are distributed in-homogeneously. Region 1, 2, 3, 4 belongs to top, middle, lower and advanced side's lower part of stir zone respectively while region 5 and 6 represent HAZ and base material microstructures.
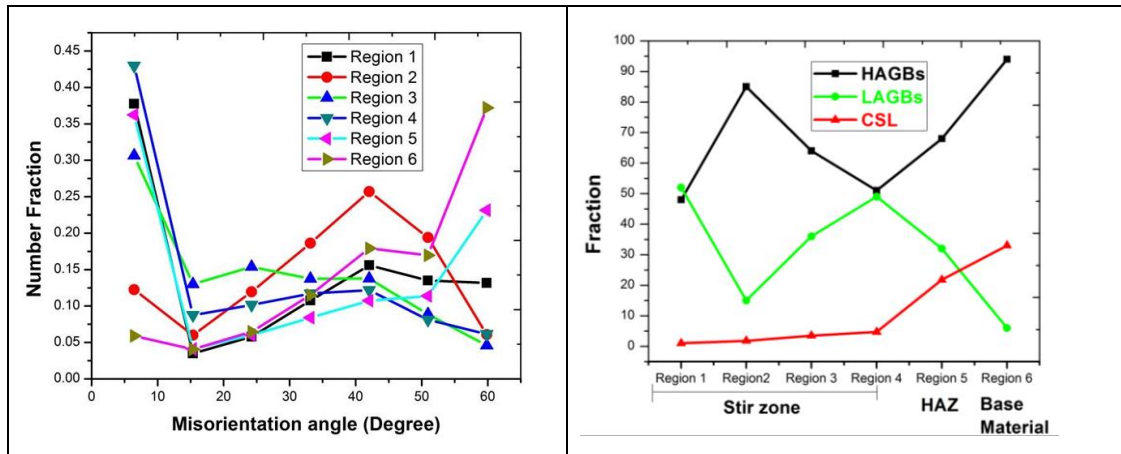
Figure 38: (a) Misorientation data derived from different regions. (b) The LAGBs, HAGBs and ∑3 twin boundary fractions for the different microstructural regions.

Table 9: The LAGBs, HAGBs and ∑3 twin boundary fractions for the different microstructural regions as shown in Figure 36

	LAGBs	HAGBs	∑3 Twin (CSL)	Grain Size
Region 1	52	48	1	36μm
Region 2	15	85	1.8	24μm
Region 3	36	64	3.5	39μm
Region 4	49	51	4.7	44μm
Region 5	32	68	21.8	48μm
Region 6 (BM)	6	94	33	27μm

Region 1-: As shown in fig 37a, the top stir zone experienced high amount of strain induced crystallographic rotation due to threaded shoulder of tool resulted in annihilation of twins into random HAGBs and generation of LAGBs. It contains nearly equal amount of HAGBs and LAGBs with only 1% of CSL boundaries. The high amount (nearly 52%) short length LAGBs indicates shear deformed microstructure. An average grain size of 36μm was observed in this region.

Region 2-: In this region HAGB formation was more pronounced. HAGB fraction reached 85% of the total grain boundary area with an average grain size of 24μm. Also, a Mackenzie type misorientation profile is obtained with maximum at 45° from this region suggesting random misoriented grain boundaries distribution which might be generated from high shear amount, ultimately resulted into small sized dynamic recrystallized grains.

Region 3-: This region is the bottom part of the stir zone showing onion rings and have experienced less deformation. The HAGB fraction is 64 % with an average grain size of 39μm, representing shear deformed region.

As we move from top to bottom of the stir zone (Region 1 to Region 3), a slight increase in the CSL boundaries (Twins) is noticed. As shear deformation eliminates twin boundaries, still the presence of low fraction of such boundaries in stir zone predicts them as to be annealing twins. Moreover, as surface material cools faster than inner region, their fraction increased from the top of the stir zone to the bottom.

Region 4-: This region contained sheared grains and belongs to onion ring on the advancing side of the region 3. Nearly equal fraction of HAGBs and LAGBs are observed and the average grain size is around 44μm. Tilted shearing from the rotating tool pin is expected in this region.

Region 5-: Near the outer edge of stir zone where the microstructure changed from the heat of the rotating pin, an average grain size of 48μm is observed. In this region only grain growth is observed with 68% HAGBs and around 29% CSL boundaries. This region was depicted as HAZ.

Region 6-: This region is base material having 94% HAGB with maximum 33% CSL boundaries and grain size of 27μm as the plates received in rolled conditions.

5.6.2 Texture analyses of Ti-6Al-4V welds

5.6.2.1 Pole Figures

Pole figures are represented in TA – ND direction of various zones of weld W1 is presented in Figure 34.
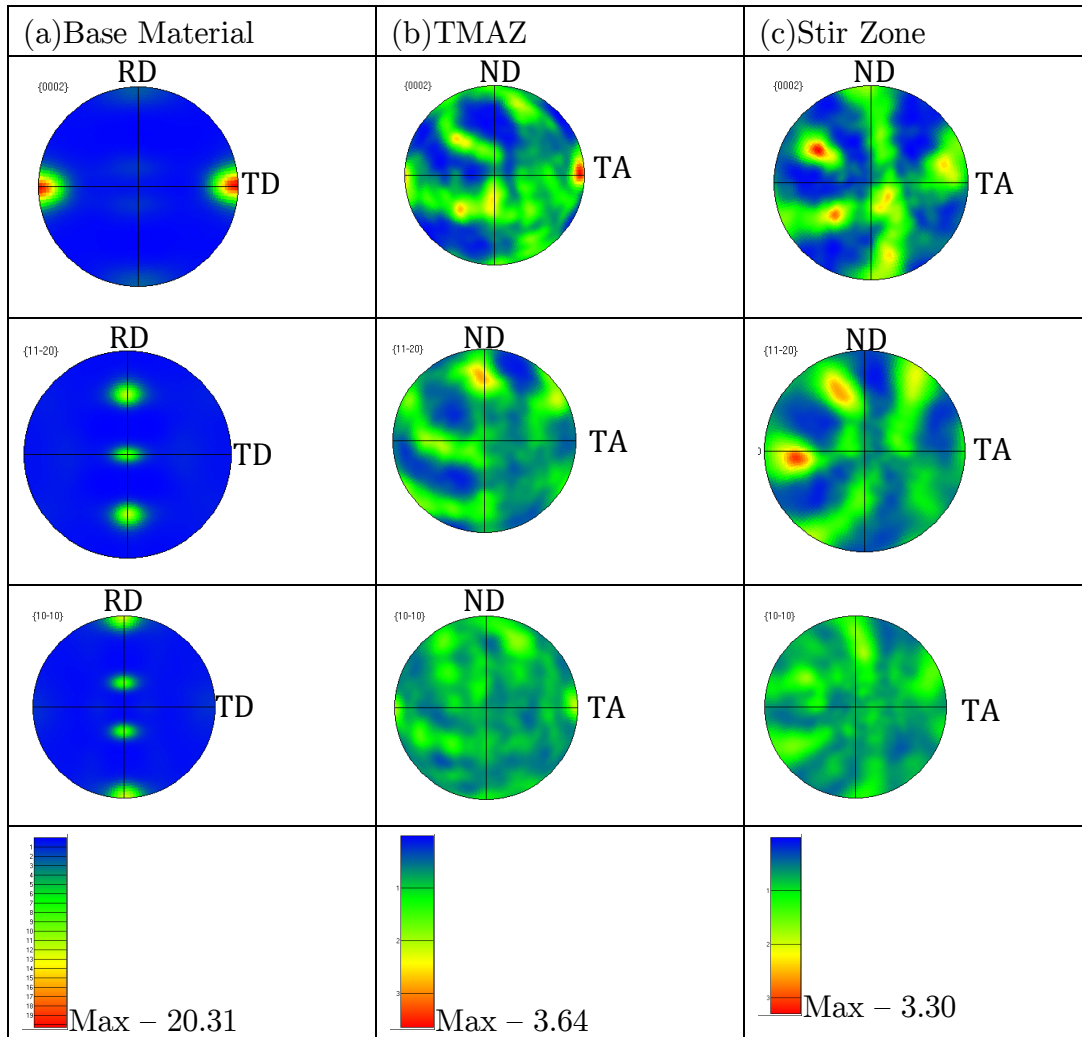
Figure 39: Pole Figure of various zones in weld W1.

(a) <u>Base Material</u> -: (0002) PF in fig 34a represent a strong basal texture along welding direction (WD) with <11-20> along the tensile axis (TA).

(b) <u>TMAZ</u> -: In this zone, with the retention of initial (0002) <11-20>, other sheared texture components are generated.

(c) <u>Stir Zone</u> -: In this zone, a tool pin rotation induced shear texture with reduced intensity is obtained.

5.6.2.3 Grain Boundary Analyses of Ti-6Al-4V

Figure 40 shows grain boundary maps of base material, TMAZ and stir zone of Ti-6Al-4V in which green color represents LAGBs and black color shows HAGBs.

(a) <u>Base Material (BM)</u>-: As received deformed base material contained equiaxed α grains with an average grain size of 43μm and 59% of HAGBs and 41% of LAGBs. From fig 41 it's clear that BM has shown high amount of LAGBs with higher fraction of low angle misorientation than SZ and TMAZ, suggest cold rolled or warm rolled condition of the as received material.

Base Material	TMAZ	Stir Zone
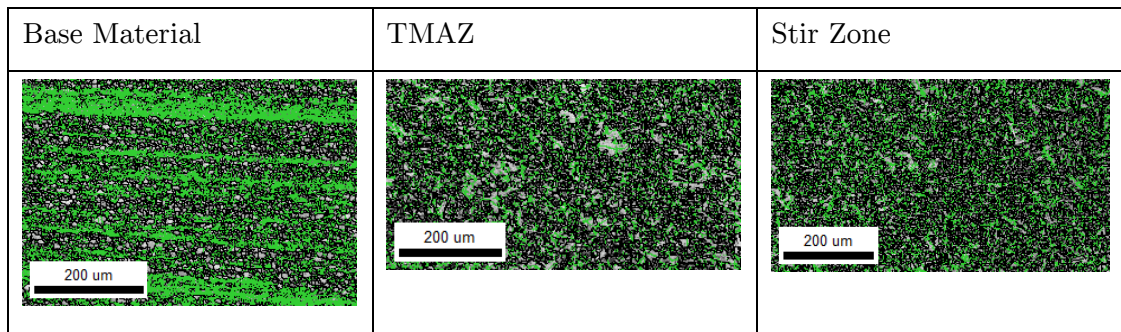
Figure 40: Grain-boundary maps showing microstructures in different regions. In the maps, LAGBs, HAGBs are depicted as green and black lines respectively.
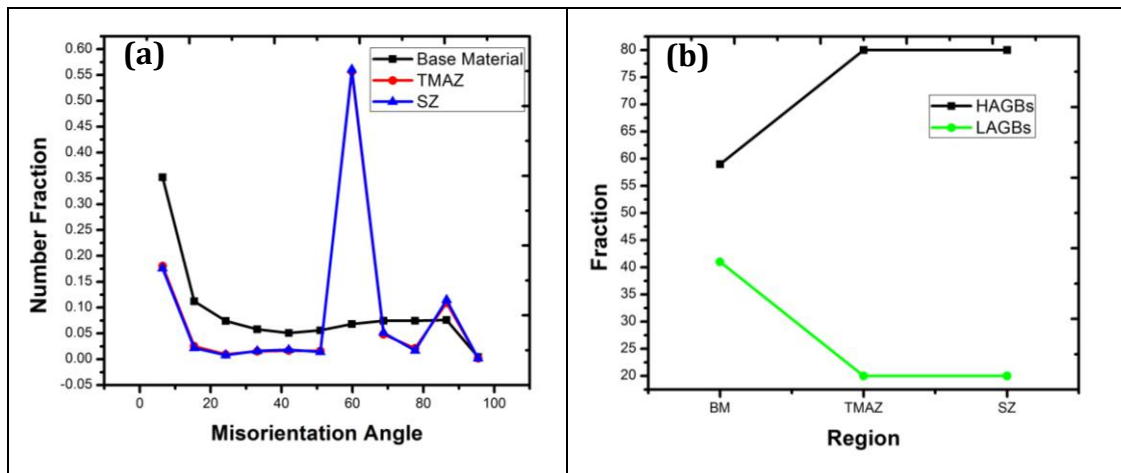
Figure 41: (a) Misorientation data derived from different regions. (b) The LAGBs and HAGBs fractions for the different microstructural regions.

(b) <u>TMAZ</u>-: Average grain size of 16μm was observed with bimodal (equiaxed primary α grains + secondary α laths) microstructure. LAGB fraction is reduced to

50

20% with misorientation at 6.45^o and HAGB fraction raised 80% having peak misorientation of 59.85^o and 86.55^o due to the transformation of β phase to secondary α lath variants. Still remaining LAGB of α phase suggests the thermomechanical microstructure change in the α+β region.

(c) <u>Stir Zone</u>-: Fine α laths with typical transformed α lath variants misorientation profile are obtained in this region suggesting stirring action in the complete β domain followed by transformation into α secondary laths during cooling.

Chapter 6

Discussion

AISI-316 and Ti-6Al-4V alloy sheets are individually friction stir welded with varying welding parameters and their welding feasibility is reported in chapter 5 through mechanical testing, hardness values, microstructure characterization, orientation mapping with grain boundary details, misorientation profiles and texture determination.

6.1 Discussion on AISI-316 welds

<u>Base Material</u> -: The base material (AISI-316), a low stacking fault energy stainless steel used for structural applications, received in sheet form consists of equiaxed austenite grains containing several annealing twins (fig. 22). Hardness value of 190 VHN and tensile strength of 608 MPa with 49% elongation are obtained in it. To predict the initial texture of the as received base material, Region 6 orientation map (fig. 33) and its associated microstructure pole figures (PF) in fig. 35 are used. Microstructure characterization through orientation map showed it of equiaxed grains of average 27μm mostly containing HAGB and Σ3 twin boundaries (table 8). Sheet shape suggest it to be rolled and equiaxed grain microstructure indicates towards cold rolled (may be +annealed) or warm rolled processing conditions. Proper Reference frame is required to analyze the obtained base material texture data. Since the as received base material is predicted to be cold or warm rolled, therefore, a rolled referenced frame (RD-TD plane) is used. Hence, for the

determination of base material texture (taken from Region 6) RD-TD reference plane is used which turned out to be TA-WD plane.

Figure 42 represents base material PF in RD-TD plane which is compared with the standard {111} PF of rolled FCC materials. Clearly, the base material is a low stacking fault energy materials and is consisted of weak brass type rolling texture with indices {110} <-112>.
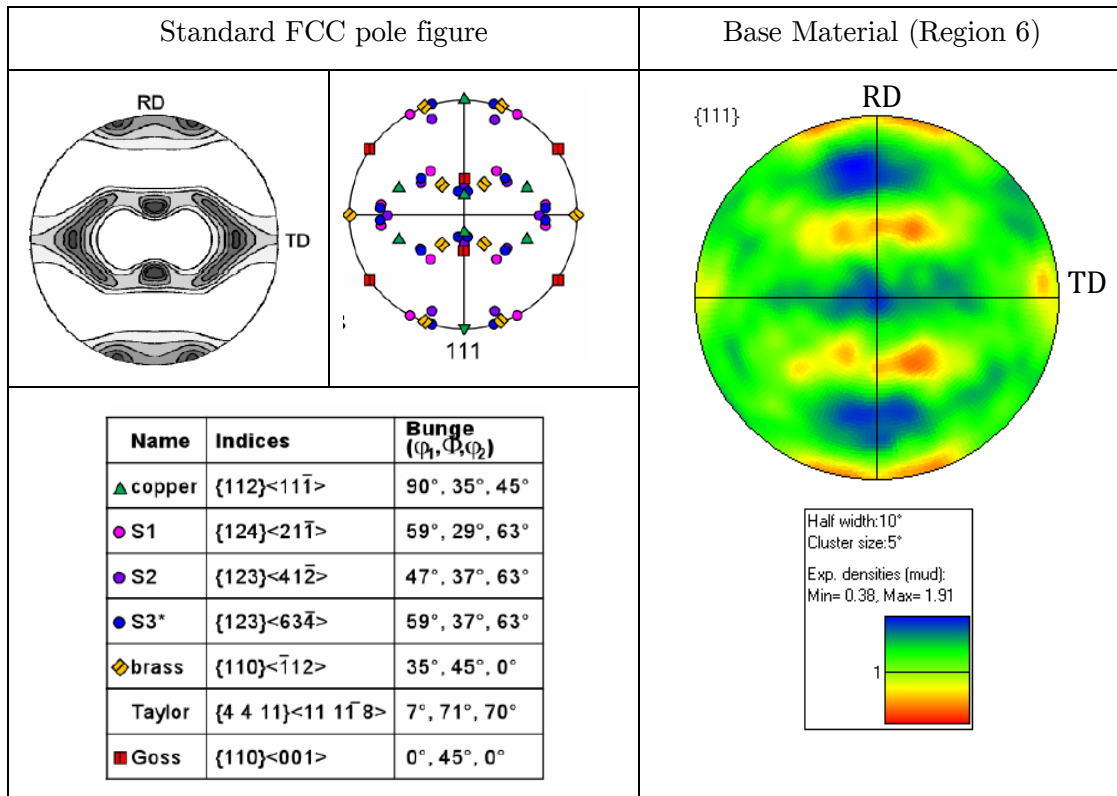
Figure 42: Standard {111} cold rolling texture of FCC materials [36] and the base material.

 T1 weld-: Sheets of dimensions 120mm x 80mm x 4mm are friction sir welded using Megastir Q70 tool. Out of all the welds with varying welding parameters, T1 weld (1100 rpm and 8mm/min welding speed) containing no processing defects, generated the best tensile test values (610MPa strength with 35% elongation). T1 necked in the base material region suggesting smooth transition of grain structure from stir zone to TMAZ, HAZ and base material region. For detailed understanding of the T1 weld, orientation map from the nugget zone towards the base material region in the advancing side is performed (fig. 33). Seeing the complexity of the microstructure in the stir zone, it is divided into top (Region 1), middle (Region 2),

bottom (Region 3) and bottom-left in the advancing side (Region 4). The HAZ is named as Region 5 and the base material as Region 6. Their grain sizes, grain misorienation profiles and texture in PFs are determined (fig 33, 35, 36, 37, 38). Stir zone is shear deformed by pin and its threads and hence contained microstructure details different than the base material. The noticed increased grain size in the stir zone regions (except in Region 2) than the base material (table 8) is mainly due to shear deformation which elongates the grains with decrease of $\Sigma 3$ twin boundaries. Region 2 containing smallest equiaxed grain size (24µm) with less $\Sigma 3$ twin boundaries than the base material is may be due to dynamic recrystallization occurred under heavy shear deformation.

To understand the shear deformation of FSW samples in the stir zone, torsion shear reference frame (Z-θ) is used. In this (Z-θ) reference frame, Z indicates the shear plane normal (SPN) and θ indicates the shear direction (SD) and generates fiber texture along these directions. In fcc, the shear is expected to occur in {111}<110> system and hence <110> tend become parallel to the SD, i.e. on θ. This tends to generate fibers {111}<uvw> fiber (also called A partial fiber) and/or {hkl}<110> fiber (also called B fiber). The locations of the ideal shear fcc texture components are shown through {100} and {111) pfs in fig. 42 with their Miller notations given in table 10. In the stir zone of FSW samples, the shear plane remains tangential to the rotating pin. Hence, at the exact middle section of the transverse plane in the stir zone, the shear plane falls exactly on the ND-TA plane. But when moving away from the middle section, the shear plane gets tangentially tilted with the tool pin surface along the ND. Therefore, to determine shear components at different places in the nugget zone, the pfs of different region are needed to be rotated to bring them into the (Z-θ) shear reference frame making <110>$_{fcc}$ ||SD. Figures 43 and 44 show the pfs (as obtained in the TA-ND reference frame and after rotation in the Z-θ shear reference frame) of four regions (Region 1 to 4) of the stir zone.

FCC {100} pole figure [Montheillet et al Acta Metall., 33, 705, 1985]	FCC {111} pole figure
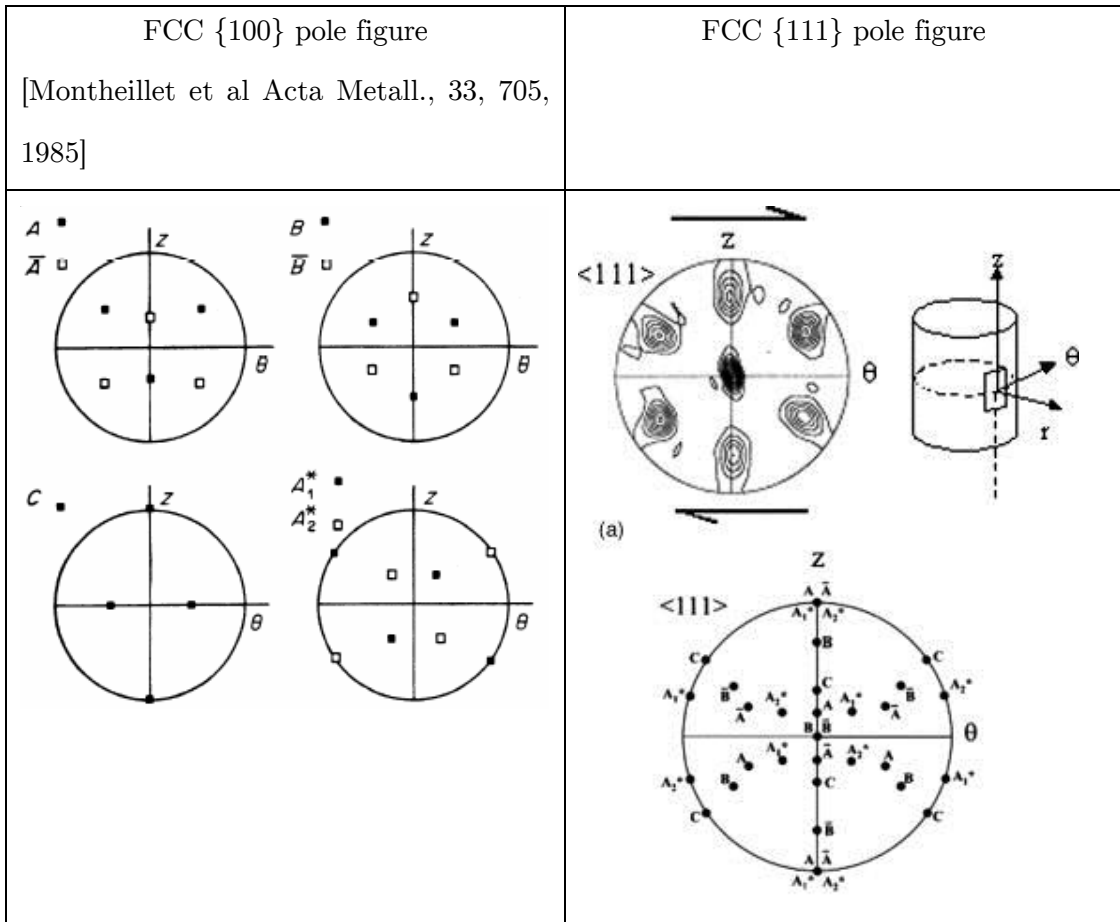
Figure 43: The standard {100} and {111} torsion sheared pole figures with shear texture components associated with FCC materials [37].

Table 10: Notation and Miller Indices used for different shear component notations.

Notation	Miller Indices
A	{1-11}<110>
$\bar{A}$	{-11-1}<-1-10>
A^*_1	{-1-11}<112>
A^*_2	{11-1}<112>
B	{1-12}<110>
$\bar{B}$	{-11-2}<-1-10>
C	{001}<110>

Region 1	Region 1 (rotated)	Region 2	Region 2 (rotated)

Max − 2.98	Rotation $(\varphi_1$ -20$^\mathbf{o}$, Φ 10$^\mathbf{o})$	Max-2.12	Rotation $(\varphi_1$ -15$^\mathbf{o}$, Φ -10$^\mathbf{o})$
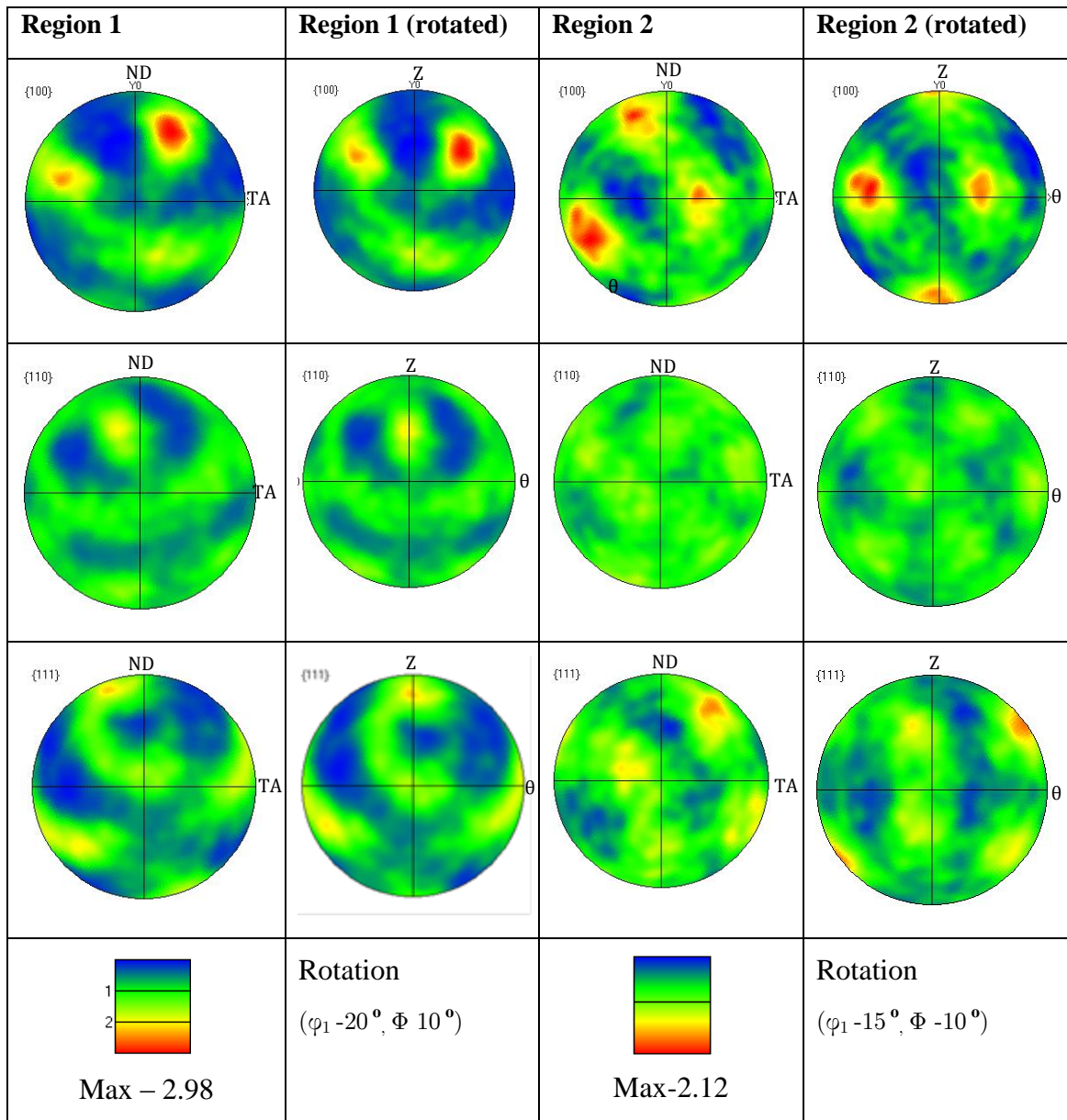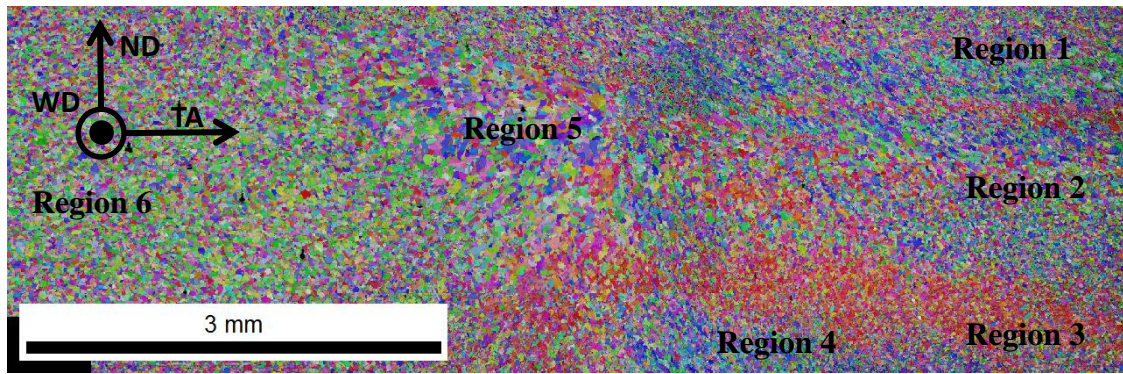
Figure 44 -: Pole Figure with and without rotation for region 1and 2 in T1 weld with IPF map.

Region 3	Region 3 (rotated)	Region 4	Region 4 (rotated)
 Max – 5.27	Rotation $(\varphi_1 - 15\,°)$	 Max- 4	Rotation $(\varphi_1 - 15\,°)$
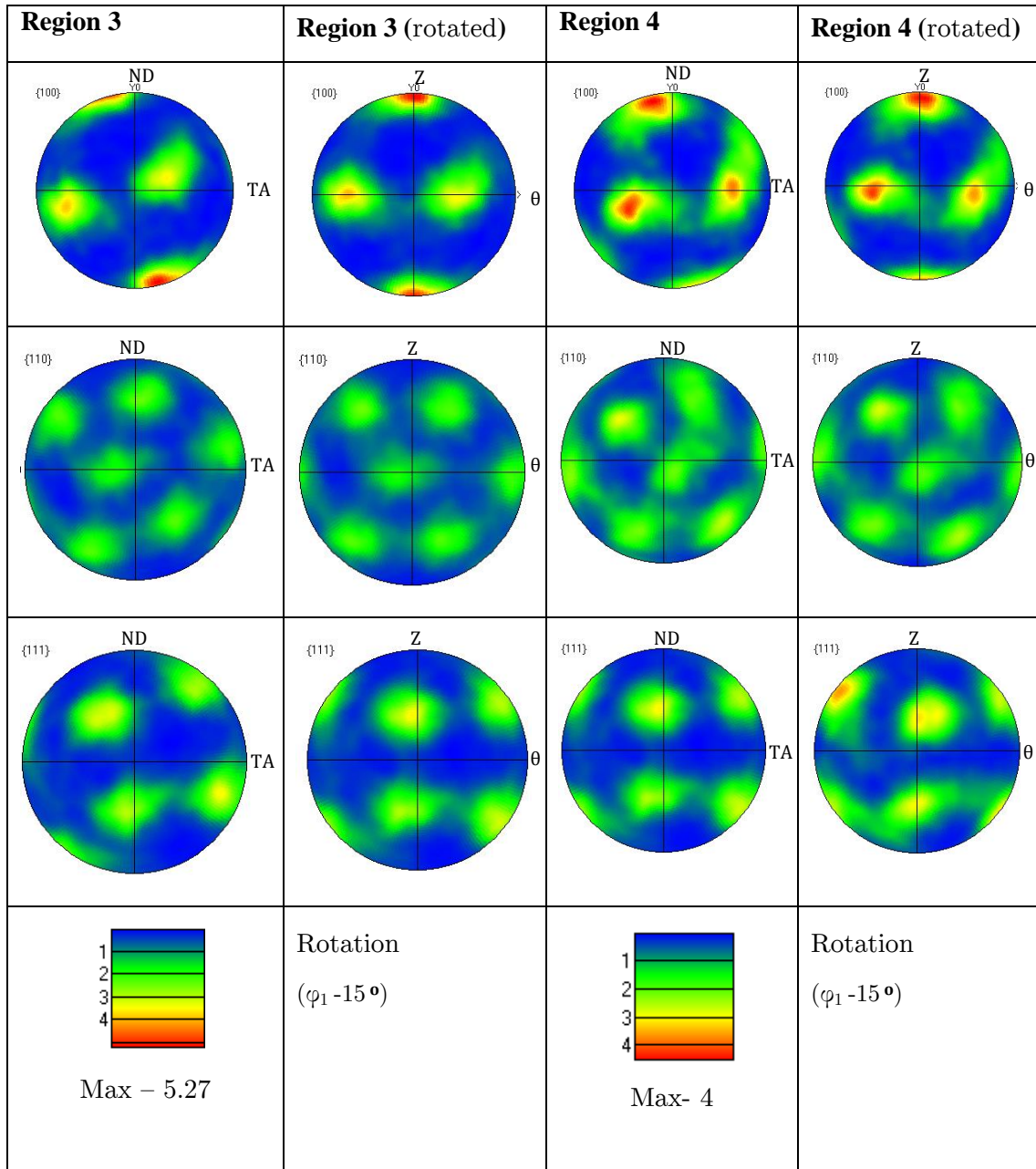
Figure 45 -: Pole Figure with and without rotation for region 3 and 4 in T1 weld.

FSW is a simple shear process in which material flows tangential to tool. The pole figures are rotated in such a way to align them in shear direction.

Region 1: To bring this region to shear reference frame the rotation $(\varphi_1, \Phi, \varphi_2)$ is given (-20, 10, 0). It is the uppermost part of the weld of advancing side showing B type partial fiber with {1-12} <110> as major shear texture component.

Region 2: Rotation given to bring PF to shear reference frame is (-15,-10, 0). It has C {001} <110> shear texture component.

Region 3: It is the Bottom most part of advancing side of weld showing strong C {001} <110> shear texture. Rotation given to for shear reference frame is (φ_1 -15).

Region 4: This region has shown C type of shear texture with Miller Indices {001} <110> when rotated φ_1 by -15° to make it in shear reference frame. The finding of C {001} <110> shear component in the stir zone (except for B {hkl} <110> partial fiber in Region 2) in the present low stacking fault stainless steel indicates predominant shear texture along the <110> direction. Earlier, Miranov et. al. [24] reported mainly A partial fiber in S31254 superaustinitic steel. C component is generally noticed in nickel (at shear 3.6) and copper (at shear 3.5) which changed to D fiber in low stacking fault brass Cu-30Zn (at shear 3.5) [36].The HAZ zone (Region 5) is situated just outside nugget zone. Its pole figure is provided in RD-TD plane and compared with ideal annealed FCC material (nickel) pole figure (fig. 46). This region shows weak tilted cube texture (100) <001>. Rolled fcc materials produce cube texture upon annealing [38].

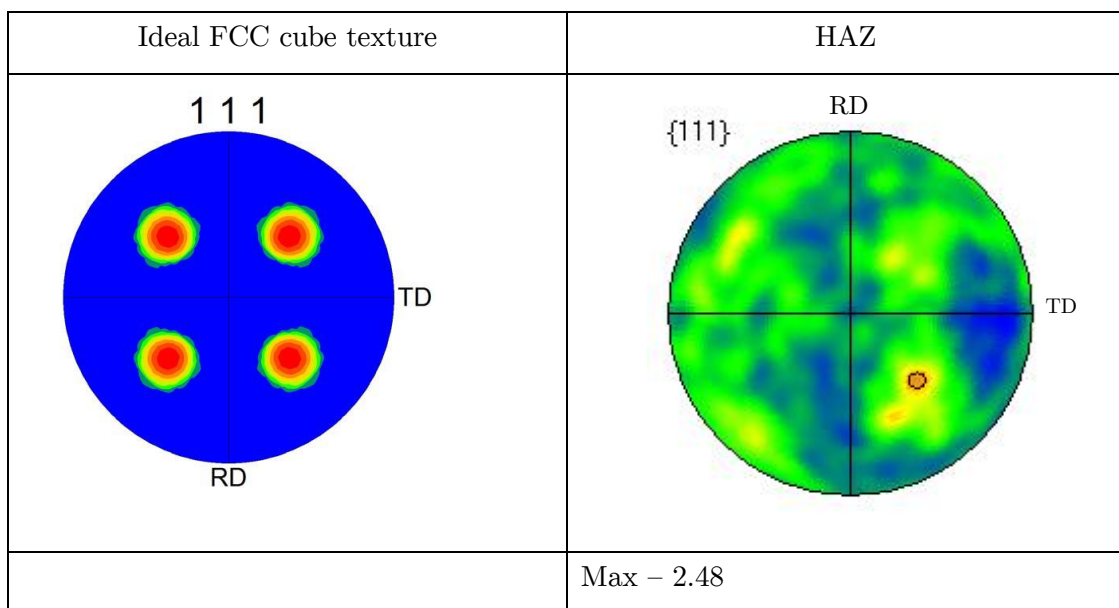| Ideal FCC cube texture	HAZ
	Max – 2.48

Figure 46 -: Ideal (111) Pole Figure in FCC material showing cube texture [38] and (111) pole figure of HAZ in T1 weld

The biggest grain size of 48μm with cube texture of the HAZ confirmed heat induced recrystallization in this region.

6.2 Discussion for Ti-6Al-4V

Base Material -: The as received Ti-6Al-4V alloy which is also used for structural applications, is obtained in sheet form consists of deformed elongated α (hcp) and β (bcc) grains (fig. 25), representing cold rolled or warm rolled microstructure. An average hardness value of 330 VHN (varied values among α and β grains) and tensile yield strength of 773 MPa with 12% elongation (table 7) are obtained in it. Like AISI 316, to predict the initial texture of the as received base material, orientation map (fig. 34) and its associated microstructure pole figures (PF) in fig. 39 are used. Microstructure characterization through orientation map showed it having equiaxed α grains of average 43μm with equal LAGB and HAGB (fig. 40, 41). Since the as received base material is predicted to be rolled, therefore, a rolled referenced frame (RD-TD plane) is used. Hence, for the determination of base material texture (taken from fig. 39) RD-TD reference plane is used which is the TA-WD plane.
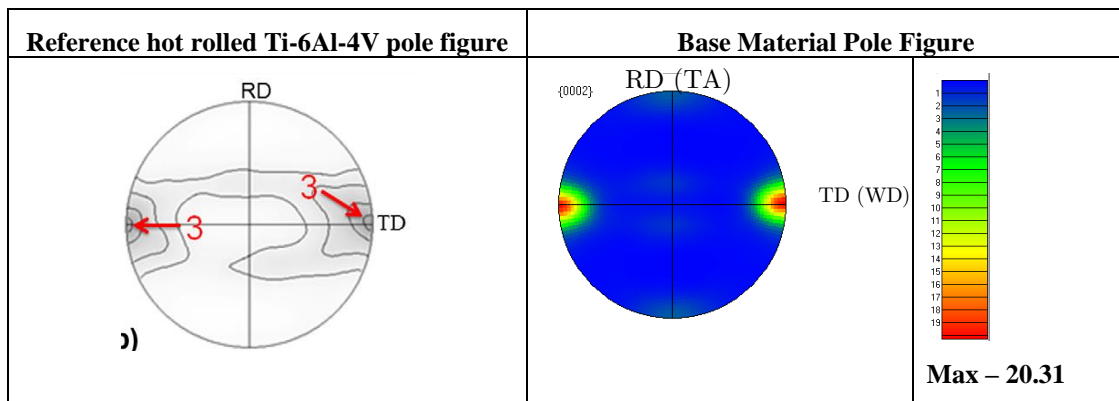
Figure 47 -: Ideal rolled [35] and as received Ti-6Al-4V plates pole figure

A figure 47 show base material PF in RD-TD plane and is compared with the (0002) PF of hot rolled Ti-6Al-4V material [35]. The Base material contained strong transverse basal texture and matches well with the reference texture.

W1 weld-: Sheets of dimensions 120mm x 80mm x 4mm are friction sir welded using Megastir Q70 tool. Out of all the welds with varying welding parameters, many showed comparable tensile yield strength but none produced interesting

elongation values. W1 and W3 welds showed no processing defects in the optical images and w1 is taken for further orientation detailing. A variation of microstructure is noticed, for eg. Nugget zone fully containing secondary α laths in the matrix β phase grains to TMAZ containing mixture of primary α grains and secondary α laths in the matrix β phase grains and finally to the deformed primary α grains. All the welds necked and fractured in the nugget zone where fine lamellar Widmanstätten secondary α laths in the matrix β phase grains are observed due to transformation from high β transus temperature.

Orientation map of W1 weld was performed and two regions (Stir Zone and TMAZ) were taken for further understanding. The stir zone containing secondary α laths with typical transformed α lath variants misorientation profile indicates the pin stirring reaching the complete β domain followed by transformation into secondary α laths during cooling. And the mixture of primary α grains and secondary α laths in the TMAZ denotes reaching of α+β region only. Since the shear occurred in the single β phase so the α pfs should be compared with the β phase shear texture. Since α and β maintains an orientation relationship, so the $(0002)_{\alpha}$ is equivalent to the $\{110\}_{\beta}$. The standard β phase shear texture $\{110\}$ pf is given in fig. 48. Also, since simple shear is the deformation mechanism in the stir zone, therefore, the pfs (fig. 39) are needed to be rotated to bring them to the shear reference frame (Z-θ) (fig. 49) and then to be compared with the standard β phase shear texture.

In this (Z-θ) reference frame, Z indicates the shear plane normal (SPN) and ϑ indicates the shear direction (SD) and in bcc, the shear is expected to occur in $\{110\}<111>$ crystallographic slip system. The rotations of these pfs are made such amount that $<11\text{-}20>||$SD and $<1100>||$SPN.

$(0002)_{HCP} \parallel \{110\}_{BCC}$
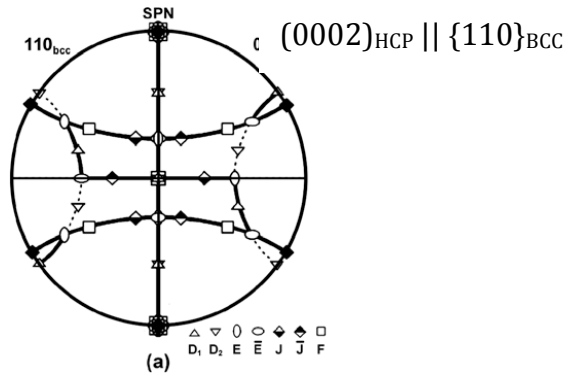
Figure 48: Schematic (110) bcc pole figure showing the main texture component orientations and fibers associated with simple shear deformation of bcc metals (Li et al.[34]).

Stir zone	Shear reference frame	TMAZ	Shear reference frame
 Max − 3.30	Rotation (φ_1 15, Φ -30, φ_2 -15)	 Max − 3.64	Rotation (φ_1 -35, Φ -20)
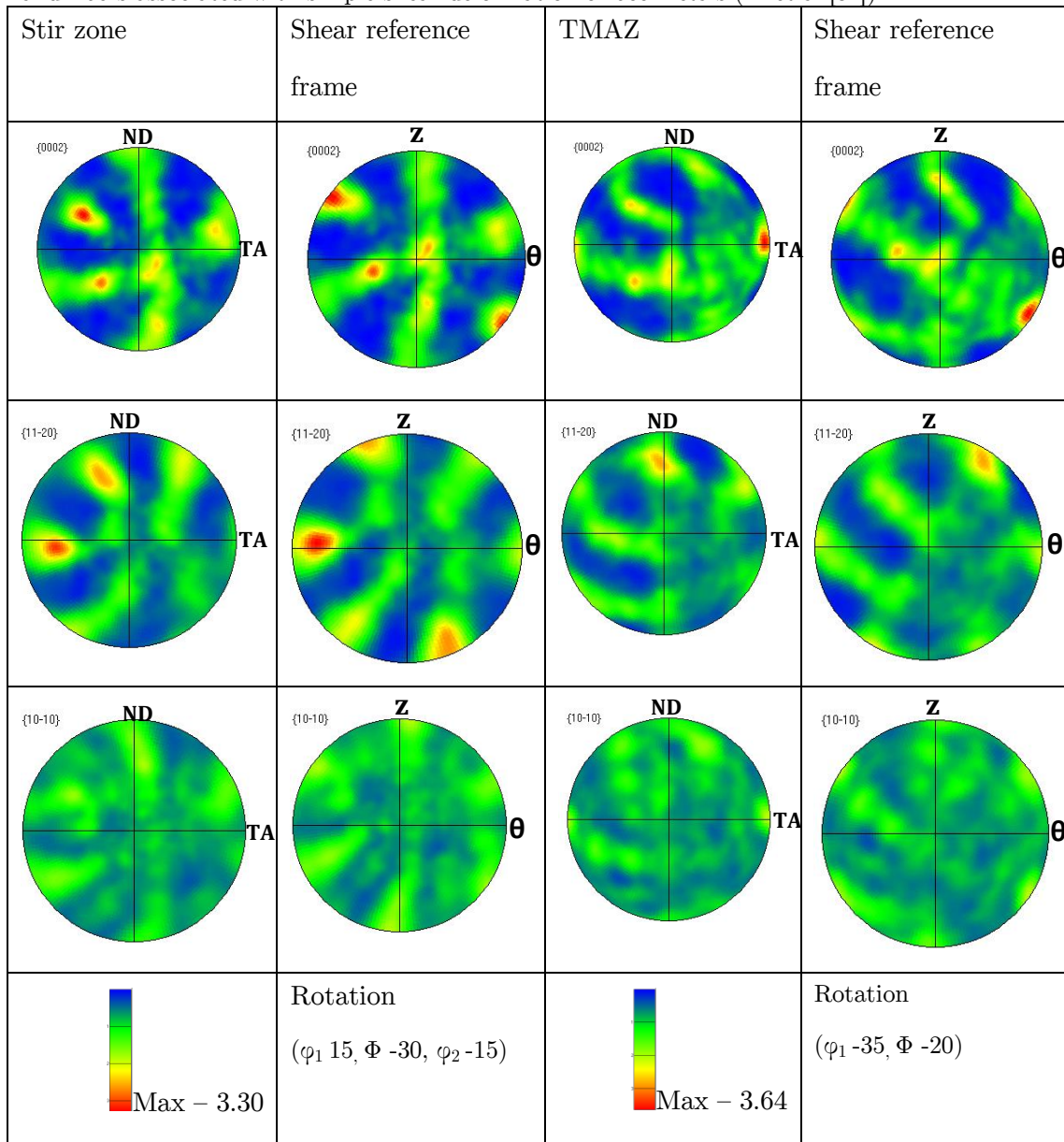
Figure 49: Pole figure of SZ and TMAZ in ND-TA plane and Shear reference frame of W1 weld

Stir Zone: The {0002} pole figure of stir zone in ND-TA plane were rotated to align with SPN –SD plane which showed D_2 {-1-12} <111> shear texture. Similar texture component has been obtained by Fonda et. al. [39] in near-α titanium alloys.

TMAZ: Since the shear occurred in the mixture containing single β (bcc) and α (hcp) grains, a combined two phase shear texture is expected and hence becomes complicated to be judged.

Chapter 7

Conclusions

1) The microstructural and mechanical evolution of AISI-316 stainless steel during friction stir welding is studied. A defect free weld is obtained with welding parameters of rotation speed <u>1100 RPM</u> and welding speed of <u>8 mm/min</u>. Ultimate tensile strength of this welded sample is obtained just above the base material with an increase in hardness in the nugget zone.

2) In stir zone original annealing twin boundaries deviate from ideal $\sum 3$ twin/matrix orientation relationship and transformed into random HAGBs.

3) C {001} <110> shear component in the stir zone (except for B {hkl} <110> partial fiber in Region 2) in the present low stacking fault stainless steel indicates predominant shear texture along the <110> direction.

4) The microstructural evolution of Ti-6Al-4V during friction stir welding is studied. A defect free weld is obtained with welding parameters of rotation speed <u>800 RPM</u> and welding speed of <u>50 mm/min</u>. In Nugget Zone, Widmanstätten secondary a laths in the matrix β phase grains, indicating its phase transformation from the high temperature β region. Whereas TMAZ consisted of deformed α grains and β transformed secondary laths, indicating its operation in the α+β region.

4) D_2 {-1-12} <111> shear texture was observed in Stir Zone of Ti-6Al-4V welds.

5) Ti-6Al-4V welds have shown around 75% of weld strength as compared to base material with minimal elongation of 2 %. This clearly shows non-feasible welding of Ti-6Al-4V with Q70 Megastir tool.

References

[1] Robert W. Messler Jr, Joining of Materials and Structures, Butterworth Heinemann, 2004.

[2] Sindo Kou. Welding Metallurgy. Second Edition. A John Willey & Sons, 2003.

[3] W.M. Thomas, E.D. Nicholas, J.C. Needham, M.G. Murch, P. Templesmith, C.J. Dawes, G.B. Patent Application No.9125978.8 (December 1991).

[4] Daniela Lohwasser, Zhan Chen, Friction stir welding from basics to applications. Wood head, 2010.

[5] Rajiv S. Mishra, Z.Y. M, Materials Science and Engineering R 50 (2005) 1–78.

[6] A. J. Bard and L. R. Faulkner. Electrochemical Methods Fundamentals and Applications. 2nd edition. John Wiley & Sons, 2001.

[7] C. Meran, O.E. Canyurt, Journal of Achievements in Materials and manufacturing Engineering, 43 (2010) 432-439.

[8] Kevin J. Colligan, Welding Fundamentals and Processes, ASM Handbook, 6A 2011.

[9] Christian B. Fuller, Friction Stir Welding and Processing, ASM Internationals, 2007.

[10] O. Frigaad, O. Grong, O.T. Midling, Metallurgical and Materials Transaction A 32 (2001) 1189-1200.

[11] Y.J. Chao, X. Qi, Journal of Materials Processing and Manufacturing 7 (1998) 215-233.

[12] W.J. Arbegast, P.J. Hartley, Proceedings of the Fifth International Conference on Trends in Welding Research, Pine Mountain, GA, USA, June 1–5, (1998) 541.

[13] T. J. Lineret, W.L. Stellwag, JR., B. B. Grimmett, R. W. Warke, Suppliment to the Welding Journal (2003) 1-9.

[14] C. Meran, V. Kovan, A. Alptekin, Materialwissenschaft und Werkstofftechnik. 38 (2007) 829-835.

[15] T.J. Lienert, J.E. Gould, in: Proceedings of the First International Symposium on Friction Stir Welding, California, (1999).

[16] E. Almanza-Casas, M.J. Perez-López, R. Steel, S. Packer, Proceedings of the Twenty-first International Offshore and Polar Engineering Conference. IV (2011) 530-533.

[17] A.P. Reynolds, Wei Tang, T. Gnaupel-Herold, H. Prask, Scripta Materialia, 48 (2003) 1289–1294.

[18] Y.S. Sato, T.W. Nelson, C.J. Sterling, R.J. Steel, C.-O. Pettersson, Materials Science and Engineering A 397 (2005) 376–384.

[19] Kumar V. Jata, Friction Stir Welding and Processing II, TMS (The Minerals, Metals & Materials Society), 2003.

[20] Won-Bae Lee, Chang-Young Lee, Woong-Seong Chang, Yun-Mo Yeon, Seung-Boo Jung, Materials Letters, 59 (2005) 3315 – 3318.

[21] H. K Bhadeshia, D. H., R. Nandan, T. DebRoy, Progress in Materials Science, 53 (2008) 980-1023.

[22] P. D. Edwards, M. Ramulu, Science and Technology of Welding and Joining, 14 (2009) 476-483.

[23] Y. Zhang, S. Yutaka, Y. S. Sato, H. Kokawa, C. Park, Satoshi Hirano, Materials Science and Engineering A, 488 (2008) 25–30.

[24] S. Mironov, Y. Zhang, Y.S.Sato, H. Kokawa, Scripta Materialia, 59 (2008) 27-30.

[25] N. Kumar, J. Rodelas, R. S. Mishra, Friction stir welding and processing V, (2009) 45-53.

[26] W.S. Miller, L. Zhuang, J. Bottema, A.J. Wittebrood, P. De Smet, A. Haszler, A. Vieregge, Materials Science and Engineering, 280 (2000) 37–49.

[27] S. D. Meshram, T. Mohandas, G. M. Reddy, Journal of Materials Processing Technology, 184 (2007) 330–337.

[28] Kaio Niitsu Campo, Leonardo Contri Campanelli, Luciano Bergmann, Jorge Fernandez dos Santos, Claudemiro Bolfarini, Materials and Design, 56 (2014) 139–145.

[29] M. Fazel-Najafabadi, S.F. Kashani-Bozorg, A. Zarei-Hanzaki, Materials and Design, 32 (2011) 1824–1832.

[30] Jinsun Liao, Naotsugu Yamamoto, Hong Liu, Kazuhiro Nakata, Materials Letters, 64 (2010) 2317–2320.

[31] J. Perrett, J. Martin, J. Peterson, R. Steel and S. Packer, TMS Annual Meeting 2011. 27 Feb. - 3 March 2011, San Diego, CA., USA.

[32] E. M. Savitskii, M. A. Tylkina, 1959. Izv. Akad. Nauk SSSR, Otd. Tekh. Nauk, Metall. Toplivo, No. 3 (1959) 99-102.

[33] V. V. Skorokhod, O. G. Radchenko, I.V. Uvarova, V.V. Panichkina, Powder Metallurgical Metal Ceramics 22 (1983) 900-903.

[34] S. Li, I.J. Beyerlein, M.A.M. Bourke, Material Science and Engineering A 394 (2005) 66.

[35] G.C. Obasi, S. Birosca 1, D.G. Leo Prakash, J. Quinta da Fonseca, M. Preuss. Acta Materialia 60 (2012) 6013–6024.

[36] A. D. Rollet, S. I. Wright Texture and Anisotropy, Cambridge University Press 1998.

[37] Montheillet, Acta Materialia 33 (1985) 705.

[38] P.P. Bhattacharjee, N. Tsuji and R.K. Ray Metallurgical and Materials Transactions A, 42 (2011) 2769-2780.

[39] K.E. Knipling and R.W. Fonda, Scripta Materialia 60 (2009) 1097–1100.